Elsevier Editorial System(tm) for Earth and Planetary Science Letters
Manuscript Draft

Manuscript Number:

Title: Particle size distributions in chondritic meteorites: evidence for pre-planetesimal histories.

Article Type: Letters

Keywords: chondritic meteorites; chondrules; CAIs; planetesimals; protoplanetary disks; asteroids

Corresponding Author: Dr. Justin I. Simon, PhD

Corresponding Author's Institution: NASA Johnson Space Center

First Author: Justin I. Simon, PhD

Order of Authors: Justin I. Simon, PhD; Jeffrey N Cuzzi, PhD; Kaitlyn A McCain, B.S.; Michael J Cato, B.S.; Peter A Christoffersen, M.S.; Kenton R Fisher, M.S.; Alastair W Tait, PhD; Danny M Olson; Jeffrey D Scargle

Abstract: Magnesium-rich silicate chondrules and calcium-, aluminum-rich refractory inclusions (CAIs) are fundamental components of primitive chondritic meteorites. It has been suggested that concentration of these early-formed particles by nebular sorting processes may lead to accretion of planetesimals, the planetary bodies that represent the building blocks of the terrestrial planets. In this case, the size distributions of the particles may constrain the accretion process. Here we present new particle size distribution data for Northwest Africa 5717, a primitive ordinary chondrite (ungrouped 3.05) and the well-known carbonaceous chondrite Allende (CV3). Instead of the relatively narrow size distributions obtained in previous studies (Ebel et al., 2016; Friedrich et al., 2015; Paque and Cuzzi, 1997, and references therein), we observed broad size distributions for all particle types in both meteorites. Detailed microscopic image analysis of Allende shows differences in the size distributions of chondrule subtypes, but collectively these subpopulations comprise a composite "chondrule" size distribution that is similar to the broad size distribution found for CAIs. Also, we find accretionary 'dust' rims on only a subset (~15-20%) of the chondrules contained in Allende, which indicates that subpopulations of chondrules experienced distinct histories prior to planetary accretion. For the rimmed subset, we find positive correlation between rim thickness and chondrule size. The remarkable similarity between the size distributions of various subgroups of particles, both with and without fine grained rims, implies a common size sorting process. Chondrite classification schemes, astrophysical disk models that predict a narrow chondrule size population and/or a common localized formation event, and conventional particle analysis methods must all be critically reevaluated. We support the idea that distinct "lithologies" in NWA 5717 are nebular aggregates of chondrules. If ≥cm-sized aggregates of chondrules can form it will have implications for planet formation and suggests the sticking stage is where the preferential size physics is operating.

Suggested Reviewers: Harold C Connelly

Rowan University
connollyh@rowan.edu
Expert on chondritic meteorites, esp. chondrule formation

Julie Paque
Caltech
paque@gps.caltech.edu
Expert on chondritic meteorites, esp. their components

Dante Lauretta
The University of Arizona
Lauretta@lpl.arizona.edu
Expert on early solar system objects and asteroids

Romy Hanna
University of Texas at Austin
romy@jsg.utexas.edu
Recently published a relevant paper in EPSL

Conel Alexander
Department of Terrestrial Magnetism
calexander@carnegiescience.edu
Expert early solar system, published a relevant paper with Steve Desch ASU (who would also be a good reviewer).

Jon Friedrich
Fordham University
friedrich@fordham.edu
Would be good reviewer, but possibly conflicted? Denton Ebel, NHM would be in a similar situation (good, but maybe conflicted)

Opposed Reviewers:

National Aeronautics and
Space Administration

**Lyndon B. Johnson Space Center**
2101 NASA Road 1
Houston, Texas 77058

February 5th, 2018

Dr. Frederic Moynier
Editor of *Earth and Planetary Science Letters*

**RE: Manuscript submission**

Dear Fred Moynier:

We have submitted our manuscript, entitled: "**Particle size distributions in chondritic meteorites: evidence for pre-planetesimal histories.**" for consideration by *Earth and Planetary Science Letters.*

In this contribution, we report new particle size distribution data for Northwest Africa 5717, a primitive ordinary chondrite (ungrouped 3.05) and the well-known carbonaceous chondrite Allende (CV3). Instead of the relatively narrow size distributions obtained in previous more limited studies, we observed broad size distributions for all particle types in both meteorites. Detailed microscopic image analysis of Allende shows that initial differences in the size distributions of chondrule subtypes existed, but that collectively these subpopulations comprise a composite "chondrule" size distribution that is similar to the broad size distribution found for CAIs.

The results are evaluated in light of current accretion scenarios, and imply a common aerodynamic size sorting process building larger aggregates of solids, the existence of which may help avoid the problematic m-km sized upper limit of many planetesimal formation models. Chondrite classification schemes, astrophysical disk models that predict a narrow chondrule size population and/or a common localized formation event, and conventional particle analysis methods must all be critically reevaluated.

We believe that this work is fundamental to understanding planetesimal formation. Please let me know if I can provide any additional information.

Sincerely yours,

Justin I. Simon

(On behalf of the coauthors)

Contact information for seven suggested reviewers:
We suggest a number of possible reviewers whose specialize span astrophysical disk formation and/or meteoritics.

[1] Dr. Harold C. Connolly Jr.

Department of Geology, Rowan University
Phone: +1 (865) 256-5261, Email: connollyh@rowan.edu

[2] Dr. Julie Paque
Division of Geological and Planetary Sciences, Caltech
Phone: +1 (626) 395-6155, Email: paque@gps.caltech.edu

[3] Dr. Dante Lauretta
Lunar & Planetary Laboratory, The University of Arizona
Phone: +1 (520) 626-1138; Email: Lauretta@lpl.arizona.edu

[4] Dr. Jon Friedrich
Department of Chemistry, Fordham University
Phone: +1 (718) 817-4446, Email: friedrich@fordham.edu

[5] Dr. Conel Alexander
Carnegie Institution of Washington, Department of Terrestrial Magnetism
Phone: +1 (202) 478-8478, Email: calexander@carnegiescience.edu

[6] Dr. Romy Hanna
Jackson School of Geosciences, University of Texas at Austin
Phone: +1 (512) 471-0260, Email: romy@jsg.utexas.edu

[7] Dr. Steve Desch
Arizona State University
Phone: + (480) 965-7742, Email: steve.desch@asu.edu

[8] Dr. Denton Ebel
American Museum of Natural History
Phone: (212) 769-5381, Email: debel@amnh.org

Highlights:

The fact that particle size distributions in both lithologies of NWA 5717 and Allende are very similar in shape after scaling to a common mean size implies the existence of a common, possibly universal, aggregation process. Ultimately, if size-selective aerodynamic effects allow particle sticking to proceed to larger aggregation sizes than currently expected, the primary formation of planetesimals becomes much easier.

# Particle size distributions in chondritic meteorites: evidence for pre-planetesimal histories.

J. I. Simon[1], J. N. Cuzzi[2], K. A. McCain[*3,a], M. J. Cato[*4,b], P. A. Christoffersen[*5,c], K. R. Fisher[*6,d], P. Srinivasan[*7,b], A. W. Tait[*8], D. M. Olson[9], J. D. Scargle[2].

[1]Center for Isotope Cosmochemistry and Geochronology, ARES, EISD-XI3, NASA Johnson Space Center, Houston, TX 77058, USA (justin.i.simon@NASA.gov).
[2]NASA Ames Research Center, Moffett Field, CA 94035, USA.
[3]The University of Chicago, Chicago, IL 60637, USA.
[4]Western Carolina University, Cullowhee, NC, 28723, USA
[5]St. Lawrence University, Canton, NY, 13617, USA
[6]University of Cincinnati, Cincinnati, OH, 45219, USA.
[7]Rutgers University, Piscataway, NJ, 08854, USA.
[8]Monash University, Clayton, 3168, VIC, Australia.
[9]BAERI, inc., Petaluma, California 94952, USA
*former summer interns at JSC through Lunar and Planetary Institute or NASA Co-op Programs

[a]now at University of California, Los Angeles, Department of Earth, Planetary, and Space Sciences, Los Angeles, CA, 90095, USA.
[b]now at University of New Mexico, Department of Earth and Planetary Sciences, Albuquerque, NM, 87131, USA.
[c]now at Centre for Planetary Science and Exploration, Department of Earth Sciences, University of Western Ontario, London, Ontario, Canada, N6A 3K7.
[d]now at ARES, NASA Johnson Space Center, Houston, TX, 77058, USA.

## Abstract

Magnesium-rich silicate chondrules and calcium-, aluminum-rich refractory inclusions (CAIs) are fundamental components of primitive chondritic meteorites. It has been suggested that concentration of these early-formed particles by nebular sorting processes may lead to accretion of planetesimals, the planetary bodies that represent the building blocks of the terrestrial planets. In this case, the size distributions of the particles may constrain the accretion process. Here we present new particle size distribution data for Northwest Africa 5717, a primitive ordinary chondrite (ungrouped 3.05) and the well-known carbonaceous chondrite Allende (CV3). Instead of the relatively narrow size distributions obtained in previous studies (Ebel et al., 2016; Friedrich et al., 2015; Paque and Cuzzi, 1997, and references therein), we observed broad size distributions for all particle types in both meteorites. Detailed microscopic image analysis of Allende shows differences in the size distributions of chondrule subtypes, but collectively these subpopulations comprise a composite "chondrule" size distribution that is similar to the broad size distribution found for CAIs. Also, we find accretionary 'dust' rims on only a subset (~15-20%) of the chondrules contained in Allende, which indicates that subpopulations of chondrules experienced distinct histories prior to planetary accretion. For the rimmed subset, we find positive correlation between rim thickness and chondrule size. The remarkable similarity between the size distributions

of various subgroups of particles, both with and without fine grained rims, implies a common size sorting process. Chondrite classification schemes, astrophysical disk models that predict a narrow chondrule size population and/or a common localized formation event, and conventional particle analysis methods must all be critically reevaluated. We support the idea that distinct "lithologies" in NWA 5717 are nebular aggregates of chondrules. If ≥cm-sized aggregates of chondrules can form it will have implications for planet formation and suggests the sticking stage is where the preferential size physics is operating.

**Introduction**

Chondrules constitute 30-80% of primitive meteorites and have been reported to be narrowly size-sorted (*e.g.,* Dodd, 1976; Ebel et al., 2016; Friedrich et al., 2012; Grossman et al., 1989; Paque and Cuzzi, 1997; Rubin, 1989; Teitler et al., 2010) as compared to CAIs that make up only 1-10% and thought to be less tightly sized-sorted (Grossman et al., 1989; Hezel et al., 2008; May et al., 1999; Wurm and Krauss, 2006b). The high abundances of chondrules in primitive meteorites suggest that chondrule formation and accumulation processes were fundamental to the earliest stages of the accretion of asteroids, which provide the parent bodies for these primitive meteorites. Since terrestrial planets formed from primitive asteroids or analogous planetesimals, understanding these early stages is important for understanding planetary accretion overall.

The mineralogy, chemical, and isotopic composition of chondritic components provide important constraints on their initial formation conditions (*e.g.,* Alexander et al., 2008; Davis et al., 1990; Davis et al., 2017; Gooding and Keil, 1981; Huang et al., 2012; Richter et al., 2002; Shahar and Young, 2007; Simon and DePaolo, 2010; Simon et al., 2017; Young et al., 2002; Yu and Hewin, 1998). However, the characteristic distributions of particle sizes in primitive meteorites likely reflect a combination of how the various subgroups of particles initially formed, at different times and in different locations in the solar nebula, and how they were preserved and/or were concentrated (i.e., sorted) between formation and parent body assembly.

There are a number of hypotheses for the formation of chondrules. Most postulate that they originated from melting early-formed dust by either localized or nebula scale energetic events in the gas-rich stage of the protoplanetary disk (Boss, 1996; Connolly and Love, 1998; Grossman et al., 1989; Jones et al., 2000), such as magnetic flares (Levy and Araki, 1989), current sheets (Joung et al., 2004), lightning (Desch and Cuzzi, 2000), impacts on or between primitive planetary bodies

(Johnson et al., 2015; Asphaug et al., 2011), nebular shock waves (Desch and Connolly, 2002; Morris and Desch, 2010; Wood, 1996), or in planetesimal bow shocks (Ciesla and Hood, 2002; Ciesla et al., 2004; Hood, 1998; Hood and Horanyi, 1993; Morris et al., 2012; Weidenschilling et al., 1998).

The more refractory mineralogy of CAIs implies that they formed from precursor materials that condensed out of nebula gas at a high temperature (Grossman et al., 2002), perhaps closer to the protoSun, or at an earlier, hotter nebula stage. There is evidence from radioisotopic age constraints that CAIs might be as much as ~2 Ma older than chondrules (Amelin et al., 2002; Connelly et al., 2012; Kita et al., 2005; Villeneuve et al., 2009). Given the significant compositional differences (implying that they formed under very different conditions) and their likely age differences, the problem of how CAIs with high-temperature minerals ultimately end up mixed with chondrules and other lower temperature minerals remains a mystery (cf. Ciesla 2010; Desch et al. 2017). These 'lucky' CAIs avoided being lost into the Sun or otherwise destroyed in the varied chaotic environments extant in the protosolar disk, including the thermal processes that produced chondrules. Partial overlap of the CAI and chondrule formation environments has been suggested, based on evidence that CAIs interacted with, and possibly some of their rims formed in a chondrule-like environment (Dyl et al., 2011; Krot et al., 2016; Simon et al., 2005; Simon and Young, 2011). Finally, the free-floating CAIs must also be 'selected' for accretion into the same planetesimal building block(s) as the chondrules.

In principle, size distributions of chondrules (Ebel et al., 2016; Friedrich et al., 2015, and references therein) and CAIs (*e.g.,* Hezel et al., 2008, and reference therein) in meteorites can be used to test astrophysical sorting processes. However, with a few exceptions (*e.g.,* Rubin, 1989; Teitler et al., 2010) the differences within and between these distinct particle groups, both of which are made up of diverse subgroups with different minerals and thermal histories, remain poorly quantified. McSween (1977) noted that CV chondrite chondrules ranged in diameter from ~550 µm to ~2000 µm. Grossman et al. (1989) reported a compiled mean diameter of ~1000 µm, but did not cite specific data sources. In abstract form, Paque and Cuzzi (1997) and May et al. (1999) reported mean chondrule diameter for CV chondrites from ~680 to 850 µm. Teitler et al. (2010) conducted a comprehensive reevaluation of the Paque and Cuzzi (1997) data, and along with additional disaggregated materials, reported mean diameters for Allende chondrules of 912 ±644 μm (n=287) and 917 ±744 μm (n=126). The available data for CAIs in Allende are more limited, but appear distinct from chondrules. McSween (1977) reported CAIs in terms of modal area fraction ranging from 2.5 to 9.4%. May et al. (1999) obtained a much smaller and narrower range between 0.65 and 1.89%. Hezel et al. (2008) found that CAIs make up 5.02±0.80% (n=223) of the modal area of three Allende thin sections, and based on these and the available literature data report that the modal area of CAIs in Allende is $2.98^{+0.3\%}_{-0.1\%}$. They also report a mean CAI diameter of ~100 μm with a pronounced peak at the smallest diameters (<100 μm). Their reported size distribution decreases monotonically to slightly larger sizes (~300 μm in diameter) and then shows a few, exceptionally large (1000's μm), outliers.

There have been a large number of size distribution studies of chondrules in ordinary chondrites. For a comprehensive view, see the excellent summary by Friedrich et al. (2015). There appears to be variability among the various chondrites (mean diameters differ from ~300 μm to ~1200 μm), but with a few exceptions, the data sets are relatively small and, like for the CV chondrites, the smallest and largest particles may have been undercounted, as discussed below.

Here we report a large-area, high-resolution study of the types and sizes of particles in the ordinary chondrite Northwest Africa 5717 (n=12,966 particles measured in a photographic mosaic) and the well-studied carbonaceous chondrite Allende (n=2339/2555 particles/particle cores measured in X-ray maps and n=6530 particles in a photographic mosaic). With this extensive data set a number of important observations can be made: (1) The measured particle size distributions are significantly broader than previously reported. This spread in size is inconsistent with previous particle sorting models (Cuzzi et al., 2001) that predict narrow size distributions. In practical terms, the differences among the measured distributions highlight the fact that sampling bias is likely a systemic problem, a problem pointed out recently (Ebel et al., 2016; Friedrich et al., 2015), and thus there is a need to reevaluate the current data and its use for defining "characteristic" particle sizes for classification purposes. (2) In Allende most (~85%) particles are unrimmed and in direct contact with meteorite host material (the matrix) whereas rims surround the other ~15%, often nearby, particles. This diverse behavior strongly argues for pre-accretional rim formation for some particles as they traversed distinct (cooler and/or dustier) nebular environments, *e.g.,* Metzler et al. (1992). (3) When present, fine-grained accretion rim types and thicknesses appear correlated to underlying particle size as recently reported for chondrules contained in the Murchison chondrite

(Hanna and Ketcham, 2017). (4) Allende shows differences in the size distributions of chondrule subtypes, but collectively these subpopulations comprise a composite "chondrule" size distribution that is similar to the broad size distribution found for CAIs. And (5) NWA 5717 contains distinct lithologies that appear to be chondrule aggregates.

**Methods**.

*Sample Materials*

Northwest Africa 5717 is an ungrouped (subtype 3.05) ordinary chondrite dominated by chondrules, that contains two apparently distinct lithologies (Bigolski et al., 2016; Bunch et al., 2010). In the studied ~11 cm x 14 cm slab, the darker of these lithologies seems to host the second, much lighter lithology (Fig. 1). The nature of the boundary between the two is variable and at times uncertain, ranging from abrupt to gradational and not always following particle boundaries. The distinction between the lithologies, beyond the obvious color differences, has been supported by a discrepancy in oxygen isotopes and an incongruity in the magnesium contents of chondrule olivine (Bunch et al., 2010). Allende is a well-studied CV3 oxidized carbonaceous chondrite that contains a range of nebular components, including a diversity of chondrule types and refractory inclusions (Fig. 2). A large piece of the Allende meteorite was cut into ~cm thick slabs and one slab was gently broken into fragments that could be mounted in one inch epoxy rounds for scanning electron microscope (SEM) analysis. SEM imagery of several unassociated Allende slab fragments were also included in this study and help ensure wide sample representation.

*Chemical phase maps, photomicrographic mosaics, and particle digitization*

Energy-dispersive X-ray chemical maps were obtained by SEM analysis of six Allende fragment samples (0.86 $cm^2$, 1.52, $cm^2$, 1.82 $cm^2$, 1.86 $cm^2$, 1.91 $cm^2$, 2.11 $cm^2$ sized pieces) using the JEOL 7600 field emission SEM at NASA Johnson Space Center. Images were acquired at 15 kV, 30 nA, with a 90 μm aperture. The images were taken at ~150x magnification with resolutions of 2.9-3.3 μm/pixel for a combined total area of 10.08 $cm^2$. Combination of characteristic X-ray emission from multiple elements was used to create chemical phase maps (maps are shown in supplemental Figs. S1-S6) in which all of the particles greater than ~50 μm in diameter were characterized. The images obtained for the Allende work were characterized by multiple investigators in a semi-blind manner detailed by Tait et al. (2016). No SEM data was acquired from NWA 5717.

Results obtained from X-ray image analyses (supplemental Table S1) were compared to results derived from a mosaic of photographic images obtained from a slab of Allende that is ~20 cm x 25 cm (supplemental Fig. S7, see Tait et al., 2016). A similar photomosaic was made for the NWA 5717 slab. To study the particles in the slabs, we photographed each using a camera attached to an optical microscope. Images were acquired in a grid pattern with a mechanical stage at a resolution of 13.9 µm/pixel. Approximately 10% overlap was used when obtaining images, which afforded accurate stitching in Adobe Illustrator. Constituent particles (*e.g.,* chondrules and CAIs) within the photomosaics were outlined in Adobe Illustrator or Photoshop using a large digitizing art board (Table S1). One side of each slab, comprised of ~300 and 400 images for NWA 5717 and Allende, respectively, was chosen for detailed analysis. Although some particles as small as ~25 µm diameter were identified, an accurate account of particles less than ~150 µm diameter in the slabs were not feasible from the photomosaics (see Discussion).

As carried out for the Allende slab photomosaic image, outlines of chondrules and CAIs were also obtained from the X-ray maps and used to create binary images of the sample particle subgroups (Fig. 3, Fig. S8). Based on the binary data, ImageJ was used to characterize the area and circularity of each individual particle and the modal area of each subgroup (Table S1). The size of each particle was calculated from the total pixels in each particle assuming a circular cross section (i.e., diameter = $\sqrt{pixel\ area/\pi} \times 2$). The lengths of the major and minor axes and orientations of individual particles were also quantified using best-fit ellipses. In general, apparent diameters calculated from best-fit ellipses match those determined from the circular cross section defined by their total number of pixels.

The "circular area definition" approach works well for chondrules, which are approximately spherical in shape and likely retain their equidimensionality even when slightly deformed (see Tait et al., 2016). This approach yields more reproducible results for the more irregular shapes of CAIs (e.g., Fig. 2), that can vary from spherical, to oblate or "pancaked" (Ivanova et al., 2014), to clumpy (i.e., "fluffy", fine-grained, and AOA type). Particles cut off by the edge of the sample were excluded because their dimensions could not be accurately measured. Additionally, for rimmed particles, we measured the apparent diameter of the inner chondrule "**core**" and the apparent diameter including the rim(s) ("**ChonMax**") so that chondrule rim thickness could be estimated by the difference. Apparent chondrule rim thicknesses were also directly measured on all particles in one of the sample SEM images (see supplemental Table S2).

*Unfolding particle size distributions from 2D area sections*

The size distributions of each particle subgroup (Table S1) were tallied, and diameter values were binned geometrically where $d_i = d_{i-1}\,c$, with $c = (d_{max}/d_{min})^{1/N}$ (starting with a bin from 0-25 μm). Regardless of binning scale, the distributions remained similar (see supplemental Fig. S9). The data sets were processed using a matrix inversion unfolding algorithm to transform histograms of measured particle diameters into histograms of actual particle diameters (Cuzzi and Olson, 2017). There are well-known sampling effects which cause the observed property $N_A(d)$, the number of particle cross sections or profiles of diameter $d$ per unit area, to differ from the more fundamental, desired quantity $N_V(D)$, the number of spheres of diameter $D$ per unit volume, *e.g.,* Eishenhour (1996). Specifically, sections tend to cut particles non-diametrically, diminishing the apparent diameter and artificially increasing the fraction at all smaller diameters, while also statistically oversampling larger particles, and at the same time overestimating fractional rim thickness (see graphical representation, supplemental Fig. S10, after Cuzzi and Olson, 2017). The algorithm has been tested using numerically "sectioned" particle samples, by comparing the diameter distribution recovered from the 2D sections to the initial 3D particle population. These tests show that meaningful and accurate unfolding of 2D area (section) data to 3D volume data can be obtained for typical meteorite particle size distributions as long as several hundred particle samples are obtained (Cuzzi and Olson, 2017).

**Results.**

*Particle types*

Subpopulations representing the diversity of particles and rims in these meteorites are defined in Table 1. Particles were initially categorized into the following subgroups: a) Porphyritic Olivine (PO) chondrules, b) Porphyritic Olivine and Pyroxene (POP) chondrules, c) Porphyritic Pyroxene (PP) chondrules, d) Aluminum-rich chondrules, e) Barred Olivine (BO) chondrules, f) melilite dominated (Type A) CAIs, g) fassaite bearing (Type B) CAIs, and h) Amoeboid Olivine Aggregates (AOA). Chondrule subgroups were considered separately and in combination so that they could be compared to the overall distribution of CAIs (including AOA). Chondrules are observed to be unrimmed, rimmed, or having two texturally distinct rim layers (an inner coarse-grained rim and an outer fine-grained rim, Fig. 2F). Chondrule data were further subdivided to account for the potential differences between size distributions of rimmed chondrules, or only their cores, to allow comparison of pre- and post-rim formation populations. Each individual particle was digitized as just a core and again including its surrounding rim, if present (see example supplemental Fig. S8).

Chondrules were grouped in several different ways to evaluate the overall distributions as categorized by: i) Maximum chondrule size (**ChonMax**), including their rims when present, j) Just chondrule cores (**AllchonCore**), i.e., treating micro-chondrule cores in rims as separate particles (see below) and excluding the additional thickness of the rims of larger particles when present, k) Cores of unrimmed chondrules (**CoreNoRim**), l) Cores of rimmed chondrules (**CoreWRim**), m) Cores of chondrules surrounded by fine-grained (**FG**) rims, and n) Cores of chondrules surrounded by fine-grained and coarse-grained (**CG**) rims. The thin Wark-Lovering (WL) and accretionary 'dust' rims on CAIs contributed negligibly to the sizes of the measured CAIs and so "naked" and rimmed CAIs were not considered separately in this work.

The small "micro-chondrules" (Fruland et al., 1978) that appear to be included within the rims themselves suggest that some of these particles either represent part of the rim formation process and/or were enveloped into a rim forming event. This complicates the counting statistics because there can be more chondrule cores ("AllchonCore" n=2555) than individual chondrules "particles" ("ChonMax" n=2339) depending on how they are defined. For this reason, we report fewer total particles when we group the instances of multiple small particle cores, embedded within large particle rims, as part of the larger particles (i.e., ChonMax as opposed to AllchonCore). Although the ChonMax and AllchonCore size distribution are similar (Fig. 5A), we consider the **ChonMax** particle population—which by definition excludes smaller particle cores contained in rims—as the most appropriate to test primary aerodynamic sorting models as earlier formed rims would contribute to the effective size of the particles during sorting.

Unfolded size distributions are shown for individual particle subpopulations in Figure 4A-J and shown overlain for comparison in Figure 5A-D. The characterization of all particles identified, both in SEM X-ray images and in photomosaics of the slabs is summarized in Table 2. Unless stated otherwise, the size distributions denote the number per unit volume of particle cores as a function of the actual unfolded geometric mean diameter without the added thickness of their associated rims. Ultimately, 13 size distribution data sets were selected for which enough data were collected to yield statistically meaningful results and for which we have confidence of accurate particle type grouping. These data sets are: (1) Maximum chondrule diameter (ChonMax, n=2339) that includes the added thickness of rims when present, (2) Chondrule core diameter (AllchonCore, n=2555) regardless of whether they have rims or are in a rim, (3) Inclusion diameter (n=195) all types, (4) Chondrule core diameter of chondrules with no rims (CoreNoRim, n=2161), (5) Chondrule core diameter of chondrules with rims (CoreWRim, n=387), excluding the added thickness of their rims, (6) PO chondrule core diameter (n=1306), (7) POP chondrule core diameter (n=1042), (8) PP chondrule core diameter (n=155), and (9) Type A CAI diameter (n=156) for Allende SEM data, (10) "All particle" diameter for Allende slab (n=6530), (11) Diameter for particles contained only in the light lithology of NWA 5717 slab (n=4121), (12) Diameter for particles contained only in the dark lithology of NWA 5717 slab (n=8206), and (13) "All particle" diameter for NWA 5717 slab (n=12,966).

Results for other particle types that are less abundant have been listed in Table 2 for completeness. These include: (1) Type B CAIs (n=24), (2) Amoeboid Olivine Aggregates (n=15), (3) Al-rich chondrules (n=21), and (4) BO chondrules (n=31) from the Allende SEM images. In general, the SEM results are consistent with component particles identified in the photomosaic Allende slab sample.

Ultimately, all of the particle subgroups were combined in the photographed Allende slab analyses because we found that visual distinction between separate particle types became uncertain below ~200 μm, and was inconsistent between the multiple observers. Although CAIs in the Allende slab were generally visible against the dark matrix, the outlines of chondrules proved more difficult to delineate than in the X-ray maps and their frequency appears to have been undercounted due to selection bias at diameters less than ~150 μm. A similar apparent drop in particle counts at the smaller sizes is seen in the NWA 5717 slab data (Fig. 5C).

Modal area percentages from Allende SEM data are derived from the three main components: chondrules (ChonMax, 46.3%), inclusions (6.2%), and matrix (47.5%). The average diameter of each particle subgroup in SEM data is calculated from a nonlinear best fit lognormal curve to each distribution (Fig. 4, see supplement for details). Average diameters of these particle subgroups vary somewhat, but all populations exhibit broad size ranges. Among chondrules, PO chondrules are the most common (51%, by number), exhibit the smallest average diameter (measured diameter ~150 µm, unfolded diameter ~160 µm), and represent 6% of the total modal area. The POP chondrules are less common (41%, by number), but are on average about 3x larger (measured diameter ~400 µm, unfolded diameter ~490 µm), so make up the largest area fraction of all particles (22%). The PP chondrules are even less common (6%), but large (measured diameter ~380 µm, unfolded diameter ~460 µm) on average, and represent ~4% of the total modal area. Each of the less common chondrule types (BO and Al-rich) appears to represent about 1% of the counts and modal area, and to be relatively large (measured diameter ~700 µm) on average. Overall 2.6% by area are Type A or Type B CAIs and 3.6% are AOA. The Type A CAIs are the most common, but smaller (measured diameter ~200 µm) on average as compared to the Type B and AOA, which on average are about 2-3x larger (measured diameter ~500 to 700 µm). The latter subgroups (Type B CAIs and AOAs along with BO and Al-rich chondrules) have too few sampled particles to assume that these averages are fully representative.

It should be noted that the largest particle sizes in the Allende X-ray images and slab are similar at ~0.2 cm, which is smaller than the largest particles that have been used for compositional studies and even smaller than a few seen in some unstudied fragments of the original bulk sample used in this study. Nevertheless, recognition that these uncharacteristically large components are undercounted here, but often studied in the published literature, attests to the importance of large sample areas for statistically representative particle size distribution work.

*Particle rims*

No resolvable rims were seen in the NWA 5717 slab. This contrasts with the ~20% fraction of particles with obvious rims in the Allende slab photomosaic. The thicknesses of rims on Allende chondrules in the SEM data set were evaluated in two ways. Rim widths were estimated indirectly by subtracting ChonWRim sizes from ChonMax sizes, and directly where all individual rim thicknesses were measured in one X-ray image (n=413 particles). In the overall SEM data set and in the single image, where rim thicknesses were directly measured, chondrules with rims represented a minority of the population (~15%), similar to the Allende slab. In the SEM data, rims surround ~10% of both PO and POP chondrule groups. Of these chondrule subtypes ~5% have only fine-grained (FG) rims, ~5% have only coarse-grained (CG) rims, and ~5% have an inner coarse-grained rim overlain by an outer fine-grained rim. No examples of inner fine-grained rims were observed. POP chondrules may have slightly more FG rims (see Table S2). The direct measurements of rim widths on chondrules are shown in Figure 6, a plot of measured rim thickness versus particle core diameter. Particles without rims are not shown in Figure 6. Among the measured particles (CoreWRim) there is a positive correlation between particle core diameter and rim thickness, as suggested by Metzler et al. (1992), Morfill et al. (1998), Cuzzi (2004); Cuzzi and Hogan (2003), and Hanna and Ketcham (2017).

## Discussion

### *Broad particle size distributions are characteristic of both meteorites*

The modal areas determined here for Allende chondrules (~46%) and inclusions (6.2% total, or 2.6% if AOAs are excluded) are generally consistent with the proportions found in previous investigations (*e.g.,* Ebel et al., 2016; Friedrich et al., 2015; Hezel et al., 2008, and references therein). Because of the difficulty of distinguishing chondrule subtypes in the slab photomosaics and, through direct evidence for undercounting of smaller (≤200 μm in diameter) chondrules from comparison of the Allende X-ray image data to the Allende slab photomicroscopy data, it is clear that photomicroscopy size distribution data are not fully representative at the smallest sizes. Furthermore, based on the largest particle sizes that have been reported in the literature, we know that neither of our samples contain the very largest sizes. Despite these complications, in both types of Allende data and in both the dark and light lithologies of NWA 5717, broad, lognormal particle size distributions are found. These observations contrast sharply with most existing studies (see Ebel et al., 2016; Friedrich et al., 2015, and references therein). This suggests that there are systematic selection bias effects in previous investigations as well, which likely undercount both smaller and potentially larger sized particles to a degree that is significantly greater than in this study.

### *Potential bias in existing data sets.*

Why and how are these data different from existing data sets? The main advantage of the detailed SEM image analysis approach is that no particle larger than ~50 μm goes unaccounted or unidentified. It is not entirely clear why previous data sets derived from 2D images fail to match the new data, but it could be related to sample bias, lower spatial resolution (i.e., use of pre-field-emission scanning microscopy techniques), observer fatigue, and/or inadequate sample area investigated. Existing studies may be biased towards larger sizes because the authors used thin sections that were selected to include larger particles for measurement of elemental or isotopic compositions (Friedrich et al., 2015, and references therein). Likewise, there are other potential sources of error in the freeze-thaw disaggregation data sets (*e.g.,* Paque and Cuzzi, 1997) where chondrules had to be hand-picked. Disaggregation size data can also be incidental with the initial goal being a composition study in which larger chondrules/CAIs were selected for ease of handling. In addition to excluding the smallest particles and undercounting others (≤500 μm), the mechanical disaggregation process might also destroy smaller particles and possibly particle rims. It has been pointed out that another potential error in the freeze-thaw disaggregation data sets occurs because the 3D particles were only measured in two dimensions (Teitler et al. 2010). Some existing ordinary chondrite data may also be biased towards larger chondrules because larger particles are more likely to have survived metamorphism on the parent body than smaller particles. This should not be a significant issue for the primitive (3.05) ordinary chondrite NWA 5717 in this work.

Polygonal shaped chondrule fragments were seen, but few looked to be obviously fractured in place. These fragments could be filtered out of the chondrule data set, by excluding chondrules with circularity $\left(= 4\pi\times\frac{[area]}{[perimeter]^2}\right)$ less than some arbitrary value (*e.g.,* 0.55) where values range from 0 (infinitely elongated polygon) to 1 (perfect circle). However, these small angular particles were included in the assessment because such a data filtering process had little effect on the spread or shape of the measured particle size distributions (shown in supplemental Fig. S11) and thus the general conclusions of this study.

To further address our concerns that the broad size distributions observed were artificially produced by inclusion of small crystals and/or angular chondrule fragments rather than actual small chondrules, we specifically re-imaged the small-sized particles characterized. Although petrologic identification of ≤50 μm size particles can sometimes be tricky, Figure 7 shows several high-resolution backscatter electron SEM images representative of small particles (~100 μm) in our data set (i.e., PO chondrules). These clearly show that the small particles are not just fragments, but rather have circular boundaries and reasonable textures and mineralogy (cf. Nelson and Rubin, 2002). Some of the small sections measured will be artifacts of 2D slicing, but our unfolding calculation accounts for this. Furthermore, the proximity of some small sections to other particles (*e.g.,* Fig. 7) preclude them from being artifacts of non-diametric slices of the ≥500 particles typical of other data sets.

Some small particles are found within in the rims of larger particles (shown in Fig. 7D-F). These “micro-chondrule" particles (Fruland et al., 1978) accreted onto other larger chondrules and do not represent small particles that were accreted individually into planetesimals. By emphasizing the **ChonMax** particle sizes, as described earlier, we are effectively excluding the fraction of small particle cores embedding in larger particle rims. The extra steps to revisit the identity of small particles in the data set validates their true independent small-chondrule nature and ultimately justifies the inclusion of these particles in the reported size distributions.

*Distinct chondrule lithologies in NWA 5717*

Dark and light chondrule-rich “lithologies” contained in NWA 5717 (Bigolski et al., 2016; Bunch et al., 2010) have similar looking broad size distributions. Bunch et al. (2010) said they were identical, but our larger data set allows us to address this claim more definitively. In order to measure the similarity, or dissimilarity, of these two distributions we ran several statistical tests (see supplement for details). First, comparison of the size distribution histograms yields strong statistical evidence that they are dissimilar. Supplemental Table S3 summarizes measures of the probability that the two distributions are the same, based on two different methods, and shown as the $\log_{10}$ of the “odds ratio”, which is the probability that the samples are drawn from the same population. The first test is an estimation of the Bayesian odds ratio for the two relevant hypotheses, based on a simple root-mean square similarity measure and constant prior (Wolpert, 1995). It is arguably superior to the commonly used Kolmogorov-Smirnov (K-S) test (Press et al., 2007), but we also include K-S probabilities in Table S3. A straightforward resampling analysis (Efron and Tibshirani, 1993) is presented in the form of bootstrap means and standard deviations of the results for both methods. Both methods overwhelmingly favor the distributions having different shapes (i.e., being drawn from different populations), consistent with their discrepant oxygen isotopes and the incongruity in the magnesium contents of chondrule olivine (Bunch et al., 2010). Put another way, Table S3 says that the probability the dark and light lithology chondrules were drawn from the same population is on the order of $10^{-50}$ or smaller. This is mostly because their mean sizes are demonstrably different.

Combined with the already known chemical and isotopic differences between the dark and light lithologies (Bunch et al., 2010), these size distribution results strongly suggest that NWA 5717 likely contains an important record of two distinct kinds of chondrule aggregate, each made from chondrules formed with different properties. This in turn indicates that aggregates we see most visibly in the light lithology, but, we hypothesize, also formed the dark lithology, grew by sticking in two separate regions and/or at different times, and then diffused around as aggregates in the nebula until they accreted together into the NWA 5717 parent body and became compacted. In part, the complex internal borders between the dark and light chondrule-rich lithologies likely reflect the aggregate nature of colliding 'clumps' of particles in the nebula. Dark aggregates would have been more numerous so blended together, while the less common light aggregates stand out as "inclusions". The dark lithology appears to be darker in color because of disseminated iron staining. Preliminary Mössbauer spectra (Cato et al., 2017) provide evidence for sulfide and iron metal grains only in the light lithology and not in the dark lithology. One possible explanation of the alteration is *in situ* reaction of metal with nebular ice that originally aggregated only with the (now) dark lithology. This hypothesis is consistent with its relatively "heavy" oxygen isotopic signature (Bunch et al., 2010), along with the diffuse nature of the boundary between the two lithologies. A more thorough examination of the oxygen isotopes within individual chondrules and additional petrologic analysis of the two lithologies could provide important insight into the importance of nebular versus parent body alteration processes.

The statistical analyses also reveal that the *shapes* of the size distributions within the dark and light lithologies, once normalized to a common mean or modal size with a scaling factor (about 1.4-1.5), are the same per the powerful Wolpert analysis (see supplemental Table S4, Fig. S12a). The K-S technique is less certain that this is the case, but there are reasons to favor the Wolpert technique (Feigelson and Babu, 2017). This result could suggest that there is some kind of universality to the processes leading to the aggregation of monomer chondrules into aggregates, in what seem to be two distinct regions with rather different properties. When a similar series of statistical tests are used to compare the shape of the particle size distributions of the NWA 5717 lithologies to that of the Allende slab data we discover an intriguing result, that *all three* can be "scaled" or normalized to a universal size distribution (shown in Figs. S12b).

*Differences among petrographically distinct chondrule populations*

The remainder of our discussion focuses on the data obtained over ~10 $cm^2$ at the micrometer scale, i.e., the X-ray SEM maps. Similar size distributions of chondrules and refractory inclusions in Allende are depicted in Figure 5A. The distributions of the most abundant chondrule subgroups detailed in the SEM images are shown in Figure 5B. The largest differences seen are between POP chondrules (n=1042) that are relatively more abundant at larger sizes and PO chondrules (n=1306) that are relatively more abundant at smaller sizes. The third most abundant chondrule subgroup (PP), while noisy (Fig. 5B), defines a distribution that is nearly indistinguishable from the overall broad distributions of inclusions and chondrules (i.e., ChonMax), the latter of which is largely comprised of POP and PO chondrules. It is remarkable, but unlikely to be a coincidence, that when the POP and PO chondrule populations are considered together as one group that they exhibit nearly the same size distribution as PP chondrules and inclusions. Among the inclusion subgroups, Type A CAIs (n=156) are the most common and generally control the distribution. Many of the largest inclusions are Type B CAIs and AOAs, and therefore, both small Type B (±AOA) and large Type A CAIs, are rare and have minimal contributions to the overall distribution. For whatever reason these unobserved particle size fractions did not exist or were preferentially lost prior to particle aggregation and/or parent body accretion.

Abundance differences among petrographically distinct chondrule types have been reported in a number of chondrites. Early work by Gooding and Keil (1978; 1981) determined the percentage abundances of chondrule types from L-chondrites and concluded that size and shape are not strictly correlated with chondrule type. Nagahara (1981) obtained a similar result for ALH 77015 (L3.5). Distinct size distributions were reported for different populations in other ordinary chondrites (Gooding, 1983), but the numbers in that study were relatively small (n=141) and the conclusions may not be fully representative. Rubin and Grossman (1987) reported that in EH chondrites (n=63), Radial Pyroxene (RP) chondrules are somewhat larger than Cryptocrystalline (CC) chondrules. They also report that non-porphyritic chondrules have a broader size distribution than porphyritic chondrules and that POP chondrules are significantly larger than PP chondrules. Rubin (1989) found that in CO3 chondrites (11 samples), PO chondrules are on average larger than PP chondrules. More recently, Nelson and Rubin (2002) found that non-porphyritic chondrules are generally larger than porphyritic chondrules (n=380) in Semarkona (CO3). They concluded that this was due to preferential fragmentation of porphyritic chondrules on the parent body. It is notable that in our work on Allende chondrules, no significant difference was seen in the size distributions as a function of particle circularity, which can be used as potential index of fragmentation. For example, of the ChonMax particles, 2% have circularity <0.35 and these exhibit a measured mean diameter of 358±137 μm (2 SE), as compared to the measured mean diameter of 310±16 μm (2 SE) for all of the ChonMax chondrules.

*Chondrule rims record pre-parent body accretion history*

The fact that a majority of the particles are unrimmed, but hosted in the same meteorite with rimmed particles, supports the notion that individual chondrule subgroups retain signatures of different trajectories on which they evolved separately in space, either by condensation of vapor or by accretion of fine particles on their surfaces, prior to the final accretion event (Morfill et al., 1998). This dichotomy further supports the interpretation that discrete component particles formed and evolved in different nebular environments prior to being caught up in the final sorting regime of planetesimal accretion. A family of model curves was computed following the theoretical approach of Cuzzi (2004) where rim thickness is a function of gas drag stopping time, i.e., larger particles travel further and faster, sweeping up more dust (see Fig. S13 and supplement for modeling details). Representative "thick-rim" models that capture the positive trend between core size and rim thickness, and some that show the apparent 'leveling off' at small particle diameters (i.e., in PO chondrules), are shown in Figure 6. Within uncertainty the data and models are consistent with the work of Hanna and Ketcham (2017) on chondrule rims in Murchison, but more data are needed to fully explore potential differences between distinct chondrule subtypes within and among different meteorites.

The evidence indicating thicker chondrule rims on larger particle cores is especially robust after one takes into account the competing effects on the appearance of rim thickness due to sample sectioning artifacts. Rim thicknesses surrounding particles in SEM images tend to be sectioned non-diametrically, like the particles themselves, artificially increasing the rim width at all smaller apparent diameters. If rim thickness is uniform, it should appear thinnest, reflecting its true thickness, on diametric particle cross sections. Therefore, the observed increase in rim thickness as the size of particle cores increases actually underrepresents the increased width of rims surrounding larger particles (i.e., POP chondrules). A simple geometric sectioning model based on the difference between two concentric circles (delta of smaller core and larger rim) that demonstrates the spurious effect on apparent rim thickness in the small non-diametric sections is shown in Figure 6 (dashed curve). The random sectioning approach of Cuzzi and Olson (2017) was used to generate delta-function size distributions to more comprehensively assess these artifacts (see Fig. S14 and supplement for modeling details). This modeling indicates that some of the observed scatter is likely due to sectioning.

*Theoretical considerations of particle rimming and sorting*

Rim formation represents a finite event or events, following condensation or partial melting, during which the particle was coated by dust as it passed through a dusty gas reservoir before it was accreted by sticking into an agglomeration of particles, *e.g.,* Gooding and Keil (1981); Simon et al. (2005). The presence of coarse-grained (CG) rims, fine-grained (FG) rims, or both rim types, and varying thickness of rims observed on Allende chondrules, likely reflect time(s) when sufficient dust levels existed in the nebula to rim particles. As chondrules diffused through the nebula they likely encountered a spectrum of heating events, or at least, the ones in the rimming region did so. A common thermodynamic explanation for converting fine-grained minerals to coarse-grained ones by adding heat is Ostwald ripening, in which a dispersed mineral phase is annealed (or texturally matured). Some heating events would be too weak to have a "ripening" effect, and in this scenario the FG rim would be left alone. A stronger event could bake the FG rim to create a CG rim, and the chondrule optionally carries on to accrete a new FG rim. Whether or not a given particle was ever rimmed, it is clear that strong nebular heating was common enough to melt and/or ablate all or at least the margin of many to generate the ubiquity of "naked" chondrule cores in chondrites.

The presence of turbulence in the protoplanetary disk is one way to explain the thicker rims surrounding larger chondrule cores (Fig. 6, Hanna and Ketcham, 2017). In a turbulent regime, larger particles are predicted to move faster through gas and thus form thicker rims (Cuzzi, 2004). The observed positive correlation (Fig. 6) may also be consistent with numerical studies that suggest their formation in bipolar solar jets where chondrules ejected outwards from the protoSun impacted hypersonically with regions of dusty nebular gas (Liffman and Toscano, 2000). However, it could be explained by any scenario that exposed particles to varying dust/gas and thermal histories (*e.g.,* Connolly and Love, 1998; Morfill et al., 1998), at least for the populations of rimmed chondrules.

The distinct size distributions and rim fractions reported herein (*e.g.,* POP vs. PO), imply that the particles have most likely followed different post-formation histories and their initial size distribution(s) may well have been modified by associated sorting processes in the protoplanetary disk, prior to accretion of the parent body. Sorting processes operating in the early solar nebula have been ascribed to mass (Kuebler and McSween, 1999), differential velocities or turbulent concentration (Cuzzi et al., 2001; Cuzzi and Zahnle, 2004), photophoresis (Wurm and Krauss, 2006a), X-winds (Shu et al., 1996), density (Teitler et al., 2010), or turbulent diffusion (Jacquet et al., 2012), some or all of which may even work simultaneously. All but one of these processes rely on the size-density dependence of aerodynamic drag, and are hypothesized to occur in a number of radial mixing and transport disk models (Cuzzi et al., 2005; Jacquet et al., 2012). The general mechanism of each can be related in principle to observed size distributions (*e.g.,* Teitler et al., 2010), but this relation is not always clear, and may be complicated or overwritten by other processes.

In principle, size sorting could happen after planetesimal accretion as well (Akridge and Sears, 1999; Bland and Travis, 2017; Nelson and Rubin, 2002), but detailed petrofabric studies of the Allende slab used in this study suggest that these are of secondary importance (Tait et al., 2016). It has also been suggested that rim textures can be produced on the parent body (Allen et al., 1980; Kring, 1991; Trigo-Rodriguez et al., 2006). It is not obvious, however, how *in situ* rim formation can produce the positive rim thickness versus particle size relationship observed herein (Fig. 6) or by Metzler et al. (1992), Paque and Cuzzi (1997), Hanna and Ketcham (2017) or the layering effects observed by Bland et al. (2011), and it certainly has problems explaining the fact that only ≤20% of the chondrules in Allende measured in this study have rims.

*Evidence for nebular particle aggregation*

Why the formation of aggregates—which happens by collisions and sticking—seems to manifest some kind of (plausibly aerodynamic) sorting remains unexplained, but supporting evidence can be found in IDPs (Wozniakiewicz et al. 2012, 2013), and some hypotheses are being pursued (Cuzzi et al. 2017). The variable internal porosity of aggregates, which may decrease as they approach a bouncing barrier, affects their own aerodynamic stopping times and complicates the situation. The explanations being pursued are not narrow size "filters" but broad ones, consistent with the broad observed particle size distributions (detailed models have not yet been developed). The implication is that the particle size distribution was set during aggregate formation, not planetesimal formation as previously argued by, *e.g.,* Cuzzi et al. (2010).

Our combined findings in Allende and NWA 5717 point to a picture that has the following elements: (1) individual chondrules have an extended lifetime in the nebula as isolated objects, traversing regions with different properties (i.e., dusty regions in which fine-grained rims can be accumulated, as distinct from regions containing little or no dust; varied thermal environments that act to coarsen or eliminate the pre-existing fine-grained rims). This evolution is probably dominated by turbulent diffusion, and implies some finite radial extent of sampling that depends on nebula turbulent intensity and duration (Cuzzi et al., 2005; Cuzzi et al., 2010). (2) On some timescale that is probably longer than the rim accretion timescale (Cuzzi, 2004), based on the Allende mix of rimmed and unrimmed chondrules, chondrules collide and stick with each other, with similar-size particles of other types such as refractory inclusions if present, and maybe clusters of such objects collide with similar-size clusters, to form aggregates that reach fairly large packing fractions, which may reach a "bouncing barrier" limit after which further growth is stalled (Birnstiel et al., 2011; Estrada et al., 2016; Zsom et al., 2010). This stage may be illustrated by at least the light lithology of NWA 5717. However, small porous aggregates such as these still diffuse radially in moderate turbulence without settling, having a diffusion coefficient not much different than their constituent particles (Cuzzi and Hogan, 2003; Youdin and Lithwick, 2007; Jacquet et al., 2012). After some longer time period, associated with radial mixing across wider regions, aggregates of different types may mix and experience the kinds of conditions under which a planetesimal can form. NWA 5717 is unique in that what appear to be constituent aggregates are so qualitatively different as to be readily distinguished. We hypothesize that its dark lithology is composed of similar aggregates in greater abundance, so they simply smear together, suggesting that original (analogous) aggregates forming Allende, for instance, may be currently impossible to distinguish. In Allende, it seems there is no obvious spatial clustering of rimmed versus unrimmed chondrules, so they must have acquired their rims well before ending up in aggregates. We think it is important to test this hypothesis in other primitive chondrites.

If this scenario is correct, the observed chondrule size distributions reflect the size distributions of the components that formed aggregates by sticking, and thus may have been influenced by the probability that a particle can stick, rather than bounce. Regardless of the processes that resulted in the broad—and possibly universal—size distributions, our findings from

NWA 5717 (and likely Allende as well) suggest that chondrules can grow by sticking into aggregates of several cm size, and if verified and extended to other objects, this would have profound implications for planetesimal formation.

## Conclusions

The similar broad size distribution of particle sizes measured across particle subtypes in Allende (i.e., ChonMax and inclusions) suggests that some process size-sorted mineralogically and petrographically diverse refractory inclusions, rimless chondrules, and already-rimmed chondrules collectively prior to their incorporation into the chondrite parent body. These broad size distributions are also seen in the primitive ordinary chondrite NWA 5717, but are different between its two chemically and isotopically distinct lithologies, suggesting the patches of lithology are actually pre-planetesimal aggregates that formed in widely separated regions of the nebula and diffused together prior to planetesimal formation. Some aspect(s) of the aggregate accretion process appears to have over-printed previous, distinct size distributions that existed between particle types (*e.g.,* PO vs. POP); those due to post-formation, pre-planetesimal sorting events. The apparent positive but nonlinear correlation between chondrule size and rim thickness in Allende supports growth of at least some chondrule rims in a turbulent dusty gas reservoir. Collectively, the relatively broad, but noticeably different, lognormal size distributions of the various chondrule subtypes, as well as the presence of distinct rimmed and unrimmed chondrules in Allende, rule out mechanisms that predict single sourced, proximally formed, particle size/type populations, *e.g.,* Johnson et al. (2015). The fact that particle size distributions in both lithologies of NWA 5717 and Allende are very similar in shape after scaling to a common mean size implies the existence of a common, possibly universal, aggregation process. Ultimately, if these size-selective aerodynamic effects allow particle sticking to proceed to larger aggregation sizes than currently expected, the primary formation of planetesimals becomes much easier.

## Acknowledgments

Scientific discussions with J. M Friedrich, D. Ebel, the suggestion to explore the thick-rim regime by R. Hanna, the analytical assistance obtaining X-ray Images by D. K. Ross, and the generous loan of Allende and NWA 5717 meteorite slab samples by P. Mani and J. Minafra are greatly appreciated. L. Keller is also thanked for providing one Allende X-ray map. This work is partially supported by NASA grants 11-COS11-66 and 16-EW_2-0163 to J.I.S. and

811073.02.07.03.15, originally from NASA's Origins of Solar Systems Program, to J.N.C. NASA Cosmochemistry (11-COS11-66), Lunar and Planetary Institute internship, and NASA co-op programs supported the summer work of the 6 student authors.

**References**


Akridge, D.G., Sears, D.W.G., 1999. The gravitational and aerodynamic sorting of meteoritic chondrules and metal: Experimental results with implications for chondritic meteorites. Journal of Geophysical Research 104, 11,853-811,864.

Alexander, C.M.O., Grossman, J.N., Ebel, D.S., Ciesla, F.J., 2008. The formation conditions of chondrules and chondrites. Science 320, 1617-1619.

Allen, J.S., Nozette, S., Wilkening, L.L., 1980. A study of chondrule rims and chondrule irradiation records in unequilibrated ordinary chondrites. Geochimica et Cosmochimica Acta 44, 1161-1175.

Amelin, Y., Krot, A.N., Hutcheon, I.D., Ulyanov, A.A., 2002. Lead isotopic ages of chondrules and calcium-aluminum-rich inclusions. Science 297, 1678-1683.

Asphaug, E., Jutzi, M., Movshovitz, N., 2011. Chondrule formation during planetesimal accretion. Earth and Planetary Science Letters 308, 369-379.

Bigolski, J.N., Weisberg, M.K., Connolly, H.C.J., Ebel, D.S., 2016. Microchondrules in three unequilibrated ordinary chondrites. Meteoritics and Planetary Sciences 51, 235-260.

Birnstiel, T., Ormel, C.W., Dullemond, C.P., 2011. Dust size distributions in coagulation/fragmentation equilibrium: numerical solutions and analytical fits. Astronomy and Astrophysics 525, id.A11, 16 pp.

Bland, P.A., Howard, L.E., Prior, D.J., Wheeler, J., Hough, R.M., Dyl, K.A., 2011. Earliest rock fabric formed in the Solar System preserved in a chondrule rim. Nature Geoscience 4, 244-247.

Bland, P.A., Travis, B.J., 2017. Giant convecting mud balls of the early solar system. ScienceAdvances 3.

Boss, A., 1996. Nonaxisymmetry in the solar nebula: Disk evolution of giant gaseous protoplanet formation, Lunar and Planetary Science Conference pp. 141-142.

Bunch, T.E., Rumble III, D., Wittke, J.H., Irving, A.J., Pitt, D., 2010. Multilithologic, extra-ordinary chondrite Northwest Africa 5717: further evidence for unrecognized metal-poor, non-carbonaceous chondritic parent bodies, Lunar and Planetary Science Conference, Abst. #1280.

Cato, M.J., Simon, J.I., Ross, D.K., Morris, R.V., 2017. Examination of multiple lithologies within the primitive ordinary chondrite NWA 5717, 48th Lunar and Planetary Science Conference, Abstr. #1964.

Ciesla, F.J., 2010. The Distributions and Ages of Refractory Objects in the Solar Nebula. Icarus 208, 445-467.

Ciesla, F.J., Hood, L.L., 2002. The Nebular Shock Wave Model for Chondrule Formation: Shock Processing in a Particle—Gas Suspension. Icarus 158, 281-293.

Ciesla, F.J., Hood, L.L., Weidenschilling, S.J., 2004. Evaluating planetesimal box shocks as sites for chondrule formation. Meteoritics and Planetary Sciences 39, 1809-1821.

Connelly, J.N., Bizzarro, M., Krot, A.N., Nordlund, A., Wielandt, D., Ivanova, M.A., 2012. The Absolute Chronology and Thermal Processing of Solids in the Solar Protoplanetary Disk. Science 338, 651-655.

Connolly, H.C., Love, S.G., 1998. The formation of chondrules: petrologic tests of the shock wave model. Science 280, 62-67.
Cuzzi, J.N., 2004. Blowing in the wind: III. Accretion of dust rims by chondrule-sized particles in a turbulent protoplanetary nebula. Icarus 168, 484-497.
Cuzzi, J.N., Ciesla, F.J., Petaev, M., Krot, A.N., Scott, E.R.D., Weidenschilling, S.J., 2005. Nebular Evolution of Thermally Processed Solids: Reconciling Models and Meterorites, Chondrites and the Protoplanetary Disk. ASP Conference Series, pp. 732-773.
Cuzzi, J.N., Hartlep, T., Simon, J.I., Cato, M.J., 2017. Aggregates: The Fundamental Building Blocks of Planetesimals, 48th Lunar and Planetary Science Conference, Abstr. #1964.
Cuzzi, J.N., Hogan, R.C., 2003. Blowing in the wind: I. Velocities of chondrule-sized particles in a turbulent protoplanetary nebula. Icarus 164, 127-138.
Cuzzi, J.N., Hogan, R.C., Bottke, W.F., 2010. Towards initial mass functions for asteroids and Kuiper Belt Objects. Icarus 208, 518-538.
Cuzzi, J.N., Hogan, R.C., Paque, J.M., Dobrovolskis, A.R., 2001. Size-selective concentration of chondrules and other small particles in protoplanetary nebula turbulence. Astrophysical Journal 546, 496-508.
Cuzzi, J.N., Olson, D.M., 2017. Recovering 3D particle size distributions from 2D sections. Meteoritics and Planetary Sciences 52, 532-545.
Cuzzi, J.N., Zahnle, K.J., 2004. Material enhancement in protoplanetary nebulae by particle drift through evaporation fronts. Astrophysical Journal 614, 490-496.
Davis, A.M., Hashimoto, A., Clayton, R.N., Mayeda, T.K., 1990. Isotope Mass Fractionation during Evaporation of $Mg_2SiO_4$. Nature 347, 655-658.
Davis, A.M., Zhang, J., Greber, N.D., Hu, J., Tissot, F.L.H., Dauphas, N., 2017. Titanium isotopes and rare earth patterns in CAIs: Evidence for thermal processing and gas-dust decoupling in the protoplanetary disk. Geochimica et Cosmochimica Acta.
Desch, S.J., Connolly, H.C.J., 2002. A model of the thermal processing of particles in solar nebula shocks: Application to the cooling rates of chondrules. Meteoritics and Planetary Sciences 37, 183-207.
Desch, S.J., Cuzzi, J.N., 2000. The Generation of Lighting in the Solar Nebula. Icarus 143, 87-105.
Desch, S.J., Kalyaan, A., Alexander, C.M.O'D., 2017. The Effect of Jupter's Formation on the Distribution of Refractory Elements and Inclusions in Meteorites. Earth and Planetary Astrophysics, arXiv:1710.03809.
Dodd, R.T., 1976. Accretion of the ordinary chondrites. Earth and Planetary Science Letters 30, 281-291.
Dyl, K.A., Simon, J.I., young, E.D., 2011. Valence state of titanium in the Wark-Lovering rim of a Leoville CAI as a record of progressive oxidation in the early Solar Nebula. Geochimica et Cosmochimica Acta 75, 937-949.
Ebel, D.S., Brunner, C., Konrad, K., Leftwich, K., Erb, I., Lu, M., Rodriquez, H., Crapster-Pregont, E.J., Friedrich, J.M., Weisberg, M.K., 2016. Abundance, major element composition and size of components and matrix in CV, CO and Acfer 094 chondrites. Geochimica et Cosmochimica Acta 172, 322-356.
Efron, B., Tibshirani, R., 1993. An Introduction to the Bootstrap. Chapman and Hall, New York.
Eishenhour, D.D., 1996. Determining chondrule size distributions from thin-section measurements. Meteoritics & Planetary Science 31, 243-248.

Estrada, P.R., Cuzzi, J.N., Morgan, D.A., 2016. Global Modeling of Nebulae with Particle Growth, Drift, and Evaporation Fronts. I. Methodology and Typical Results. Astrophysical Journal 818, id.200, 241 pp.

Feigelson, E., Babu, J., 2017. Beware the Kolmogorov-Smirnov test!, Penn State Astrostatistics and Astroinformatics Portal.

Friedrich, J.M., Rivers, M.L., Perlowitz, M.A., Meinhart, Z., Ramirez, V.V., 2012. Characterization of Particle Size Standard NIST 1019b with Synchrotron X-ray Microtomography and Digital Data Extraction. Particle & Particle Systems Characterization 29, 35-42.

Friedrich, J.M., Weisberg, M.K., Ebel, D.S., Biltz, A.E., Corbett, B.M., Iotzov, I., Kahn, W.S., Wolman, M.D., 2015. Chondrule size and related physical properties: A compilation and evaluation of current data across all meteorite groups. Chemie der Erde 75, 419-443.

Fruland, R.M., King, E.A., McKay, D.S., 1978. Allende dark inclusions. Proceedings of Lunar Science Conference 9th, 1305-1329.

Gooding, J.L., 1983. Survey of chondrule average properties in H-, L- and LL-group chondrites—are chondrules the same in all unequilbrated ordinary chondrites?, Chondrules and Their Origins. Lunar and Planetary Institute, Houston.

Gooding, J.L., Keil, K., 1978. Physical properties of individual chondrules from ordinary chondrites, Meteoritics, p. p.476.

Gooding, J.L., Keil, K., 1981. Relative abundances of chondrule primary textural types in ordinary chondrites and their bearing on conditions of chondrule formation. Meteoritics and Planetary Sciences 16, 17-43.

Grossman, J.N., Rubin, A.E., Nagahara, H., Kring, E.A., 1989. Properties of chondrules, in: Kerridge, J.F., Matthews, M.S. (Eds.), Meteorites and the Early Solar System. Univ. Arizona Press.

Grossman, L., Ebel, D.S., Simon, S.B., 2002. Formation of refractory inclusions by evaporation of condensate precursors. Geochimica et Cosmochimica Acta 66, 145-161.

Hanna, R.D., Ketcham, R.A., 2017. Evidence for accretion of fine-grained rims in a turbulent nebula for CM Murchison. Earth and Planetary Science Letters 481, 201-211.

Hezel, D.C., Russell, S.S., Ross, A.J., Kearsley, A.T., 2008. Modal abundances of CAIs: Implications for bulk chondrite element abundances and fractionations. Meteoritics and Planetary Sciences 43, 1879-1894.

Hood, L.L., 1998. Thermal processing of chondrule precursors in planetesimal bow shocks. Meteoritics and Planetary Sciences 33, 97-107.

Hood, L.L., Horanyi, M., 1993. The Nebular Shock Wave Model for Chondrule Formation: One-Dimensional Calculations. Icarus 106, 179-189.

Huang, S., Farkaš, J., Yu, G., Petaev, M., Jacobsen, S.B., 2012. Calcium isotopic ratios and rare earth element abundances in refractory inclusions from the Allende CV3 chondrite. Geochimica et Cosmochimica Acta 77, 252-265.

Ivanova, M.A., Lorenz, C.A., Shuvalov, V.V., Krot, A.N., MacPherson, G.J., Bizzarro, M., 2014. Plastically-deformed igneous calcium-aluminum-rich inclusions from CV carbonaceous chondrites: clues to a nature of CAI melting events, 45th LPSC, Abst. # 2166.

Jacquet, Gounelle, M., Fromang, S., 2012. On the aerodynamic redistribution of chondrite components in protoplanetary disks. Icarus 220, 162-173.

Johnson, B.C., Minton, D.A., Melosh, H.J., Zuber, M.T., 2015. Impact jetting as the origin of chondrules. Nature 517, 339-341.

Jones, R.H., Lee, T., Connelly, H.C., Love, S.G., Shang, H., 2000. Formation of chondrules and CAIs: theory vs. observation, in: Mannings, V., Boss, A.P., Russell, S.S. (Eds.), Protostars and Planets. University of Arizona Press, Tucson, pp. 927-961.

Joung, M.K.R., Low, M.-M.M., Ebel, D.S., 2004. Chondrule Formation and Protoplanetary Disk Heating by Current Sheets in Nonideal Magnetohydrodynamic Turbulence. The Astrophysical Journal 606.

Kita, N.T., Huss, G.R., Tachibana, S., Amelin, Y., Nyquist, L.E., Hutcheon, I.D., 2005. Constraints on the Origin of Chondrules and CAIS from Short-lived and Long-lived Radionuclides, in: Krot, A., Scott, E.R.D., Reipurth, B. (Eds.), Chondrites and the Proloplanetary Disk, pp. 558-587.

Kring, D.A., 1991. High temperature rims around chondrules in primitive chondrites: evidence for fluctuting conditions in the solar nebula. Earth and Planetary Science Letters 105, 65-80.

Krot, A.N., Nagashima, K., van Kooten, E.M.M.E., Bizzarro, M., 2016. High-temperature rims around calcium-aluminum-rich inclusions from the CR, CB and CH carbonaceous chondrites, 47th LPSC, Abst. 1203.

Kuebler, K.E., McSween, H.Y.J., 1999. Sizes and masses of chondrules and metal-troilite grains in ordinary chondrites: Possible implications for nebular sorting. Icarus 141, 96-106.

Levy, E.H., Araki, S., 1989. Magnetic reconnection flares in the photoplanetary nebula and the possible origin of meteorite chondrules. Icarus 81, 74-91.

Liffman, K., Toscano, M., 2000. Chondrule Fine-Grained Mantle Formation by Hypervelocity Impact of Chondrules with a Dusty Gas. Icarus 143, 106-125.

May, E., Russell, S.S., Grady, M.M., 1999. Analysis of chondrule and CAI size and abundance in CO3 and CV3 chondrites: a preliminary study, Lunar and Planetary Science Conference, Abst. #1688.

McSween, H.Y., 1977. Petrographic variations among carbonaceous chondrites of the Vigarano type. Geochimica et Cosmochimica Acta 41, 1777-1790.

Metzler, K., Bischoff, A., Stöffler, D., 1992. Accretionary dust mantles in CM chondrites: Evidence for solar nebula processes. Geochimica et Cosmochimica Acta 56, 2873-2897.

Morfill, G.E., Durisen, R.H., Turner, G.W., 1998. An Accretion Rim Constraint on Chondrule Formation Theories. Icarus 134, 180-184.

Morris, M.A., Desch, S.J., 2010. Thermal histories of chondrules in solar nebula shocks. The Astrophysical Journal 722, 1474-1494.

Morris, M.A., Boley, A.C., Desch, S.J., Athanassiadou, T. 2012. Chondrule Formation in Bow Shocks Around Eccentric Planetary Embryos. The Astrophysical Journal 752, L27, 17 pp.

Nagahara, H., 1981. Petrology of chondrules in ALH-77015 (L3) chondrite., in: Nagata, T. (Ed.), Proceedings of the Sixth Symposium on Antarctic Meteorites, Tokyo, pp. 145-160.

Nelson, V.E., Rubin, A.E., 2002. Size-frequency distribution of chondrules and chondrule fragments in LL3 chondrites; Implications for parent-body fragmentation of chondrules. Meteoritics and Planetary Sciences 37, 1361-1376.

Paque, J.M., Cuzzi, J.N., 1997. Physical characteristics of chondrules and rims, and aerodynamic sorting in the solar nebula, 28th Lunar and Planetary Science Conference, Abstr. # 071.

Press, W.H., Teukolsky, S.A., Vetterling, W.T., Flannery, B.P., 2007. Section 14.3.3, Numerical Recipes The Art of Scientific Computing. Cambridge University Press, 3rd Edition.

Richter, F.M., Davis, A.M., Ebel, D.S., Hashimoto, A., 2002. Elemental and isotopic fractionation of Type B calcium-, aluminum-rich inclusions: Experiments, theoretical considerations, and constraints on their thermal evolution. Geochimica et Cosmochimica Acta 66, 521-540.
Rubin, A.E., 1989. Size-frequency distributions of chondrules in CO3 chondrites. Meteoritics 24, 179-189.
Rubin, A.E., Grossman, J.N., 1987. Size-frequency-distributions of EH3 chondrules. Meteoritics 22, 237-251.
Shahar, A., Young, E.D., 2007. Astrophysics of CAI formation as revealed by silicon isotope LA-MC-ICPMS of an igneous CAI. Earth and Planetary Science Letters 257, 497-510.
Shu, F.H., Shang, H., Lee, T., 1996. Toward an Astrophysical Theory of Chondrites. Science 271, 1545-1552.
Simon, J.I., DePaolo, D.J., 2010. Stable calcium isotopic composition of meteorites and rocky planets. Earth and Planetary Science Letters 289, 457-466.
Simon, J.I., Jordan, M.K., Tappa, M.J., Schauble, E.A., Kohl, I.E., Young, E.D., 2017. Calcium and titanium isotope fractionation in refractory inclusions: Tracers of condensation and inheritance in the early solar protoplanetary disk. Earth and Planetary Science Letters 472, 277-288.
Simon, J.I., Young, E.D., 2011. Resetting, errorchrons and the meaning of canonical CAI initial $^{26}Al/^{27}Al$ values. Earth and Planetary Science Letters 304, 468-482.
Simon, J.I., Young, E.D., Russell, S.S., Tonui, E.K., Dyl, K.A., Manning, C.E., 2005. A short timescale for changing oxygen fugacity in the solar nebula revealed by high-resolution Al-26-Mg-26 dating of CAI rims. Earth and Planetary Science Letters 238, 272-283.
Tait, A.W., Fisher, K.R., Srinivasan, P., Simon, J.I., 2016. Evidence for impact induced pressure gradients on the Allende CV3 parent body: consequences for fluid and volatile transport. EPSL 454, 213-224.
Teitler, S.A., Paque, J.M., Cuzzi, J.N., Hogan, R.C., 2010. Statistical tests of chondrule sorting. Meteoritics and Planetary Sciences 45, 1124-1135.
Trigo-Rodriguez, J.M., Rubin, A.E., Wasson, J.T., 2006. Non-nebular origin of dark mantles around chondrules and inclusions in CM chondrites. Geochimica et Cosmochimica Acta 70, 1271-1290.
Villeneuve, J., Chaussidon, M., Libourel, G., 2009. Homogeneous Distribution of 26Al in the Solar System from the Mg Isotopic Composition of Chondrules. Science 325.
Weidenschilling, S.J., Marzari, F., Hood, L.L., 1998. The Origin of Chondrules at Jovian Resonances. Science 30, 681-684.
Wolpert, D., 1995. Determining Whether two Data Sets are from the Same Distribution.
Wood, J.A., 1996. Processing of chondritic and planetary material in spiral density waves in the nebula. Meteoritics & Planetary Science 31, 641-645.
Wozniakiewicz, P.J., Bradley, J.P., Ishii, H.A., Brownlee, D.E., Kearsley, A.T., Burchell, M.J., Price, M.C., 2012. Grain sorting in cometary dust from the outer solar nebula. The astrophysical Journal Letters 760, L23, 26 pp.
Wozniakiewicz, P.J., Bradley, J.P., Ishii, H.A., Price, M.C., Brownlee, D.E., 2013. Pre-accretional sorting of grains in the outer solar nebula. The Astrophysical Journal 779, 164, 166pp.
Wurm, G., Krauss, O., 2006a. Concentration and sort of chondrules and CAIs in the late solar nebula. Icarus 180, 487-495.

Wurm, G., Krauss, O., 2006b. Concentration and sorting of chondrules and CAIs in the late Solar Nebula. Icarus 180, 487-495.
Youdin, A.N., Lithwick, Y., 2007. Particle stirring in turbulent gas disks: Including orbital oscillations. Icarus 192.
Young, E.D., Galy, A., Nagahara, H., 2002. Kinetic and equilibrium mass-dependent isotope fractionation laws in nature and their geochemical and cosmochemical significance. Geochimica et Cosmochimica Acta 66, 1095-1104.
Yu, Y., Hewin, R.H., 1998. Transient Heating and Chondrule Formation: Evidence From Sodium Loss in Flash Heating Simulations Experiments. Geochimica et Cosmochimica Acta 62, 159-172.
Zsom, A., Ormel, C.W., Guttler, C., Blum, J., Dullemond, C.P., 2010. The outcome of protoplanetary dust growth: pebbles, boulders, or planetesimals? IIIntroducing the bouncing barrier. Astronomy and Astrophysics 513, id.A57, 22 pp.

Table 1. Definitions

| | |
|---|---|
| CAI | Ca-, Al-rich refractory inclusion |
| AOA | Amoeboid Olivine Aggregate, a type of inclusion |
| PO | Porphyritic Olivine chondrule |
| POP | Porphyritic Olivine and Pyroxene chondrule |
| PP | Porphyritic Pyroxene chondrule |
| BO | Barred Olivine chondrule |
| RP | Radiating Porphyritic chondrule |
| C | Cryptocrystalline chondrule |
| ChonMax | chondrule of maximum particle diameter, including rim when present |
| AllchonCore | individual chondrule core, regardless of rim status -- present, absent, or co-shared rim |
| Rimmed | chondrule particle with rim, including rim |
| CoreWRim | chondrule particle with rim, excluding rim |
| CoreNoRim | chondrule particle that lacks rim |
| Type A CAI | melilite dominated CAI |
| Type B CAI | pyroxene-melilite dominated CAI |
| FG rims | fine-grained rims surrounding chondrules, likely accretionary |
| CG rims | generic coarse-grained rim surrounding chondrules, possibly igneous |
| WL rims | Wark-Lovering rims surrounding CAIs |

**Table 2. Summary of particles characterized in Allende and NWA 5717.**

| Data set | Particle | Subtype | Avg. diameter (μm) | SD (μm) | Avg. diameter (μm) | SD (μm) | Area (%) | Count |
|---|---|---|---|---|---|---|---|---|
| SEM (Allende) | Inclusions | | measured | | unfolded | | | |
| | | Type A CAIs | 216 | 270 | - | | 1.4 | 156 |
| | | Type B CAIs | 559 | 583 | - | | 1.2 | 24 |
| | | AOA | 673 | 503 | - | | 0.8 | 15 |
| | | Types A & B | 262 | 347 | - | | 2.6 | 180 |
| | | **Inclusions** | 294 | 376 | 380 | 699 | 3.4 | 195 |
| SEM (Allende) | Chondrule | | | | | | | |
| | | PO | 149 | 183 | 162 | 190 | 5.7 | 1306 |
| | | POP | 397 | 339 | 488 | 482 | 22.1 | 1042 |
| | | PP | 384 | 385 | 464 | 721 | 3.6 | 155 |
| | | BO | 623 | 384 | - | | 1.3 | 31 |
| | | Al-rich | 598 | 486 | - | | 1.0 | 21 |
| | | AllchonCore | 275 | 307 | 299 | 378 | 33.7 | 2555 |
| | | **ChonMax**[a] | 310 | 398 | 334 | 458 | 46.3 | 2339 |
| SEM (Allende, image#9) | Chondrule | | | | | | | |
| | | Rimmed | 718 | 662 | - | | | 63/413 |
| | | CoreWRim | 584 | 592 | - | | | 63/413 |
| | | AllchonCore | 366 | 368 | - | | | 350/413 |
| | | ChonMax[b] | 379 | 396 | - | | | 413 |
| Slab full section (Allende) | Particles | | 363 | 296 | 410 | 358 | 39.1 | 6530 |
| *Paque Allende set 1 (in Teitler et al., 2010)*[c] | | *disaggregation* | *881* | *421* | - | | | *276* |
| Slab partial light section (NWA 5717) | Particles[d] | | 239 | 238 | 342 | 303 | | 4121 |
| Slab partial dark section (NWA 5717) | Particles[d] | | 328 | 266 | 403 | 290 | | 8206 |
| Slab combined section (NWA 5717) | Particles[d] | | 295 | 259 | 378 | 310 | >95 | 12,966 |

[a] indicates particle outer diameter including rims that occasionally include multiple particles.

[b] sum of "naked" core plus measured rim thickness.

[c] data set included for reference.

[d] minimal rims present.

**Figure 1.** Low-resolution optical photomosaic images of: (A) primitive CV3 Allende chondrite ~20 cm x 25 cm slab and (B) primitive (subtype 3.05) ungrouped chondrite NWA 5717 ~11 cm x 14 cm slab. In NWA 5717 the dark lithology is denoted by a and light by b.

**Figure 2.** Classification scheme (after Gooding and Keil, 1981) used to categorize particles in SEM X-ray compositional images, with Mg, Ca, and Al indicated by red, green, and blue, respectively. a) Porphyritic olivine chondrule (PO). b) Porphyritic olivine and pyroxene chondrule (POP). c) Porphyritic pyroxene chondrule (PP). d) Aluminum-rich chondrule. e) Barred olivine chondrule (BO). f) Coarse-grained (CG) and fine-grained chondrule rims. g) Type A CAI, h) Type B CAI. i) Amoeboid olivine aggregate (AOA).

**Figure 3. (**A) Representative example of X-ray compositional images for one section of the Allende chondritic meteorite, with color coding as in Fig. 2. (B) digitized particles, including rim(s), and (C) ChonMax particles shown in binary image.

**Figure 4.** Nonlinear best fits of lognormal curves to unfolded size particle populations. (A-F) are Allende SEM X-ray images. Subgroup ChonMax is indistinguishable from Inclusions and AllchonCore. AllchonCore is the composite population of PP, PO, and POP that individually define distinct size distribution curves. (G-J) Allende and NWA 5717 slab (photomicrographic) data also exhibit broad distributions, but likely include artifacts of undercounting of the small particle sizes. Particles are binned geometrically where the number per bin is divided by the (variable) bin width to give the number per unit radius. The effect of non-diametric particle sectioning is corrected for in the unfolding calculations (Cuzzi and Olson, 2017).

**Figure 5**. Unfolded, actual, size distributions of major particle components of Allende and NWA 5717 meteorites. (A) Similar distributions of chondrules and inclusions in Allende are broader than the narrow range of particles disaggregated by Paque and Cuzzi (1997). (B) Distributions of petrographically distinct particle types in Allende (described in Fig. 2). POP chondrule population (blue shaded) contains significantly greater numbers of larger particles than PO chondrule population (red shaded). (C) Photomicrographic slab data of Allende and ordinary chondrite NWA 5717 compared to SEM chondrite cores (AllchonCore) and Paque and Cuzzi data. (D) NWA 5717 light lithology appears to have fewer larger particles than the dark lithology. Particle binning as in Fig. 4. Significant undercounting of smaller particle sizes in slab and disaggregation work exist.

**Figure 6**. Log-log plot of chondrule rim thickness versus particle section diameter (CoreWRim) for 1 of 6 X-ray images. Representative models after Cuzzi (2004) that capture the positive trend between core size and rim thickness are shown (solid curves, see Appendix). Dashed model curve is the computed apparent rim thickness versus particle diameter from non-diametric slices of an average ~370 μm diameter particle with a uniform 135 μm thick rim. Sectioning model curve is nearly orthogonal to the data trend. Measurement scatter reflects both some 2D sectioning effects shown by the models and precision, which is poorer at the smallest sizes. Unrimmed chondrules (n=350) in image not shown.

**Figure 7.** Representative backscattered electron and X-ray compositional images of small (~100 μm) particles included in this study. RGB color coding as in Fig. 2. Small particles have diverse grain size: (A,B) "micro"-porphyritic and (C-F) porphyritic and/or single crystal chondrules, akin to larger particles. Close proximity of particles shown in A-C attest to the validity of their small size. Particles in D-F appear contained in larger particle accretion rims.

Figures

Click here to download Figure: figures.pdf

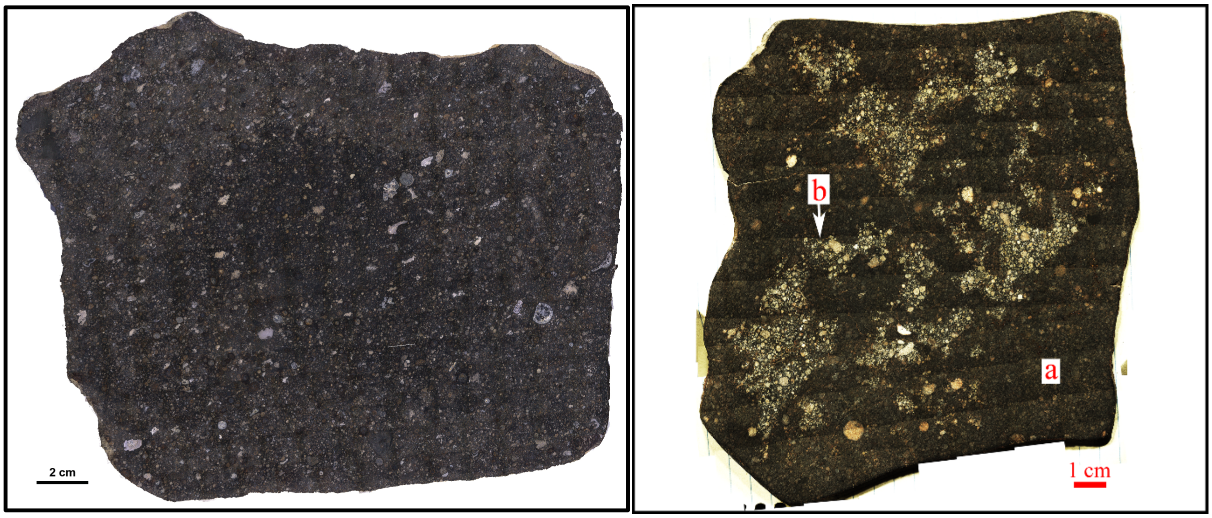


**Figure 1.**

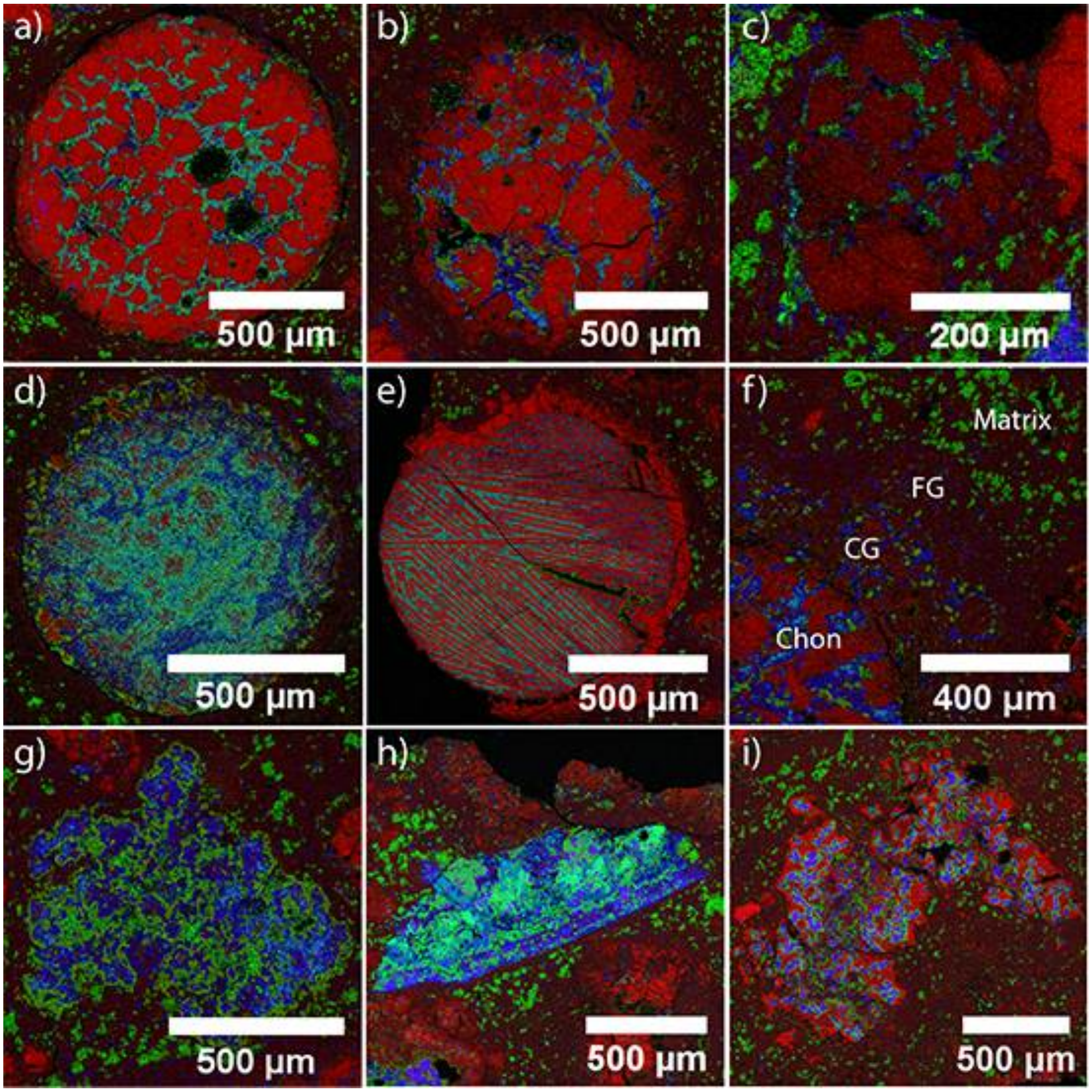
a)
500 µm
b)
500 µm
c)
200 µm
d)
500 µm
e)
500 µm
f)
Matrix
FG
CG
Chon
400 µm
g)
500 µm
h)
500 µm
i)
500 µm

**Figure 2.**

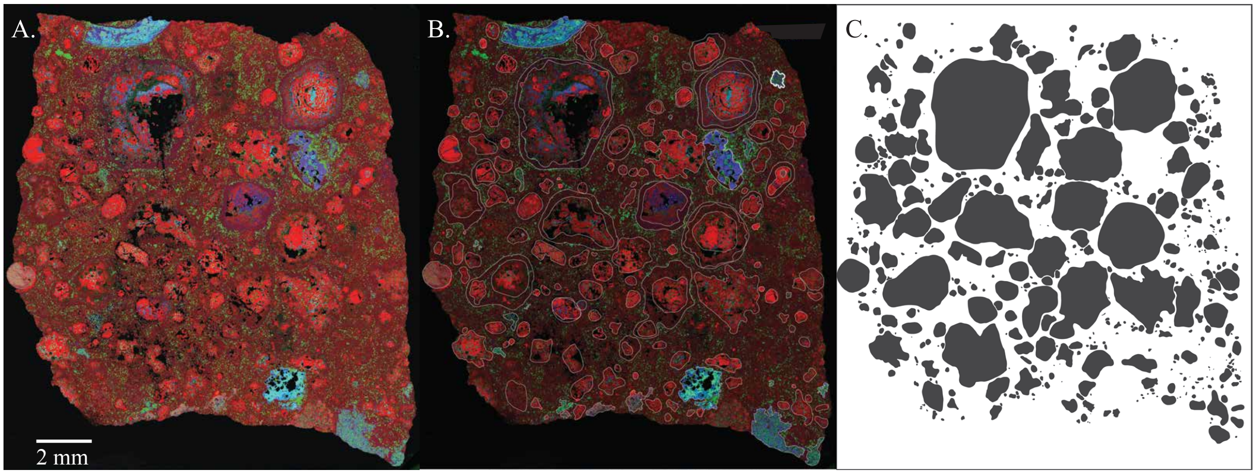


**Figure 3.**

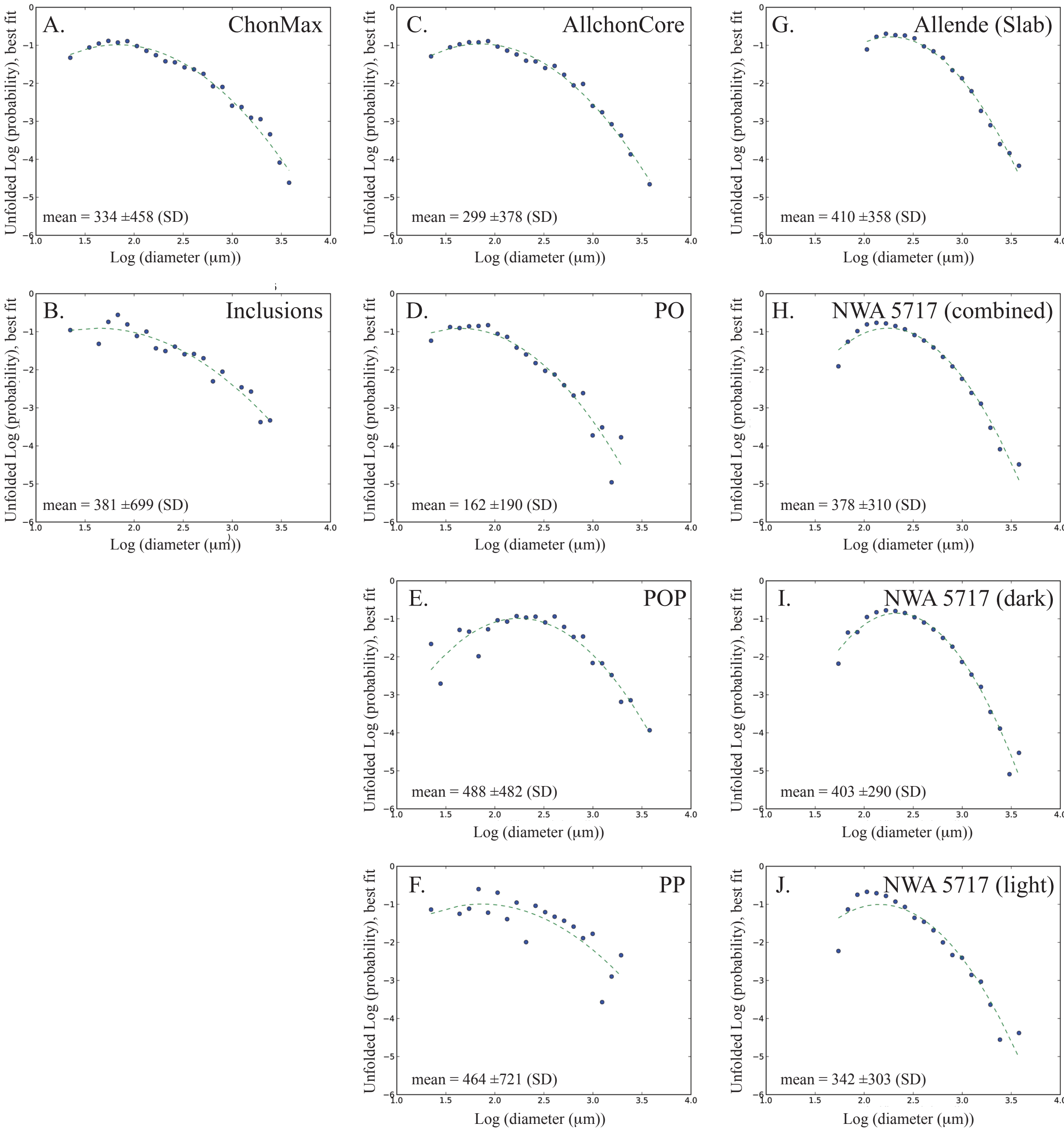
A. ChonMax
mean = 334 ±458 (SD)
C. AllchonCore
mean = 299 ±378 (SD)
G. Allende (Slab)
mean = 410 ±358 (SD)
B. Inclusions
mean = 381 ±699 (SD)
D. PO
mean = 162 ±190 (SD)
H. NWA 5717 (combined)
mean = 378 ±310 (SD)
E. POP
mean = 488 ±482 (SD)
I. NWA 5717 (dark)
mean = 403 ±290 (SD)
F. PP
mean = 464 ±721 (SD)
J. NWA 5717 (light)
mean = 342 ±303 (SD)
Unfolded Log (probability), best fit
Log (diameter (μm))

Figure 4.

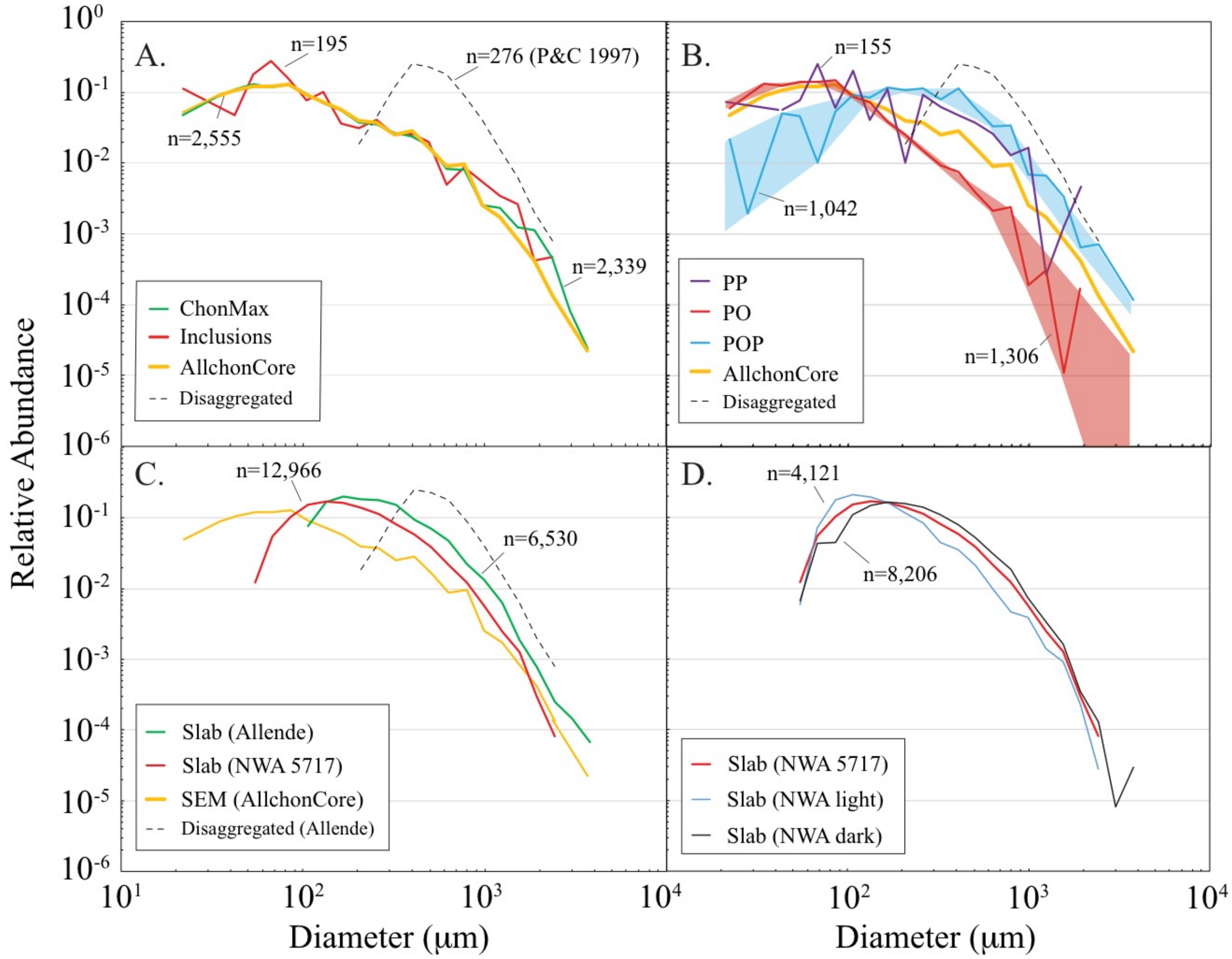
A.
B.
C.
D.
Relative Abundance
Diameter (μm)
Diameter (μm)
n=195
n=276 (P&C 1997)
n=2,555
n=2,339
ChonMax
Inclusions
AllchonCore
Disaggregated
n=155
n=1,042
n=1,306
PP
PO
POP
AllchonCore
Disaggregated
n=12,966
n=6,530
Slab (Allende)
Slab (NWA 5717)
SEM (AllchonCore)
Disaggregated (Allende)
n=4,121
n=8,206
Slab (NWA 5717)
Slab (NWA light)
Slab (NWA dark)

**Figure 5**.

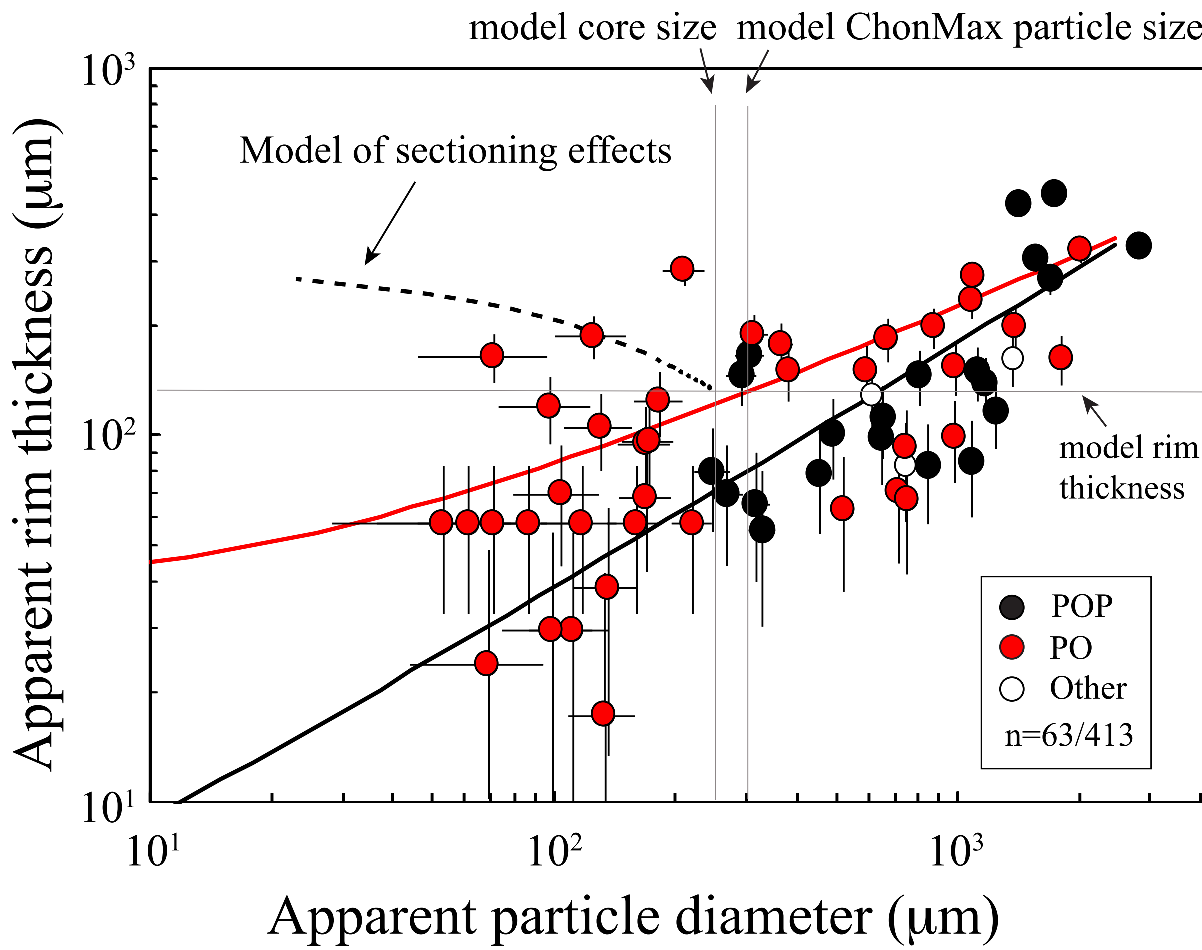
model core size
model ChonMax particle size
Model of sectioning effects
model rim thickness
POP
PO
Other
n=63/413
Apparent rim thickness (µm)
Apparent particle diameter (µm)
10³
10²
10¹
10¹
10²
10³

**Figure 6**.

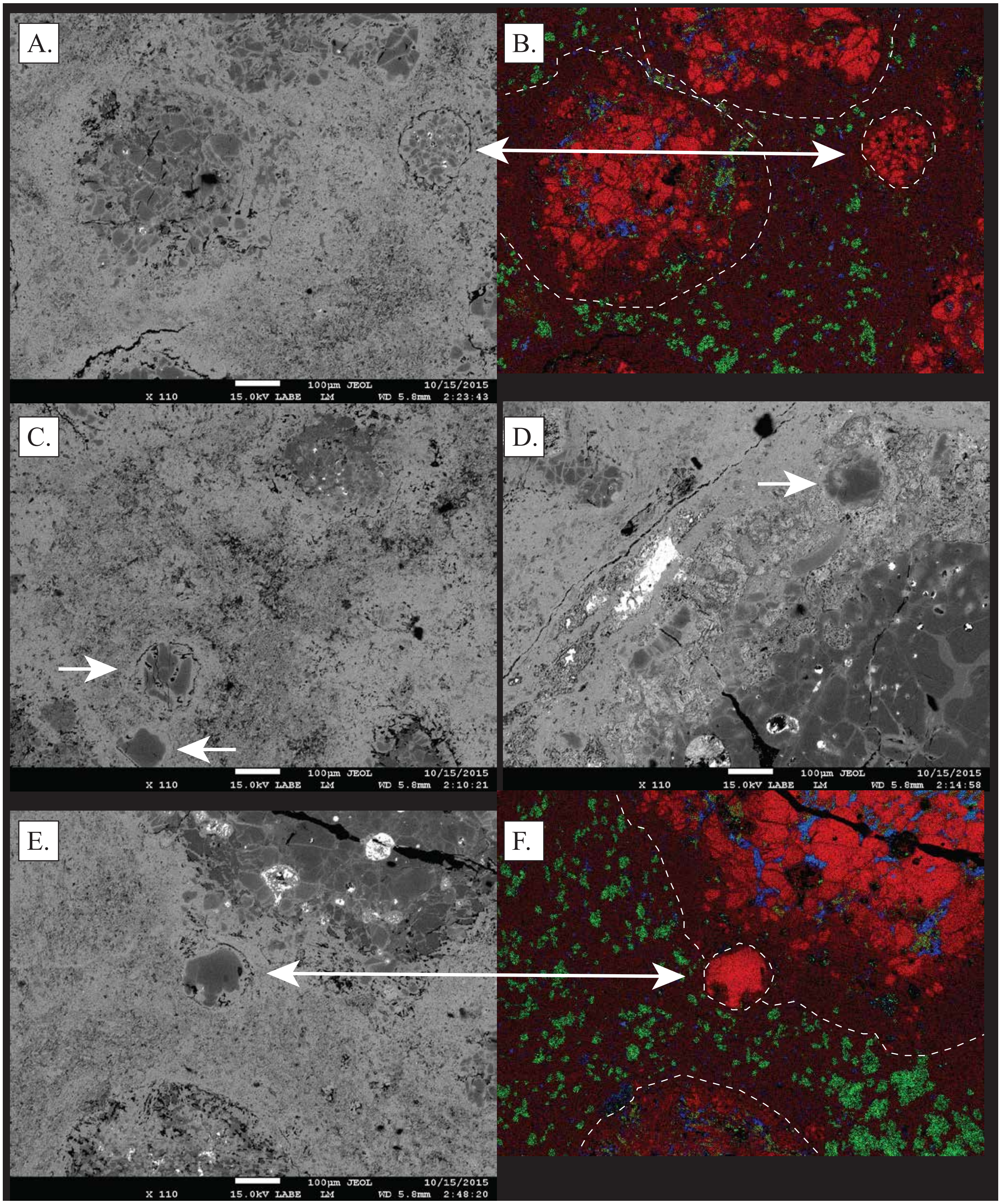
A.
B.
C.
D.
E.
F.
100µm JEOL 10/15/2015
X 110 15.0kV LABE LM WD 5.8mm 2:23:43
100µm JEOL 10/15/2015
X 110 15.0kV LABE LM WD 5.8mm 2:10:21
100µm JEOL 10/15/2015
X 110 15.0kV LABE LM WD 5.8mm 2:14:58
100µm JEOL 10/15/2015
X 110 15.0kV LABE LM WD 5.8mm 2:48:20

**Figure 7.**

**Supplementary T1**

**Click here to download Supplementary material for online publication only: Table S1.xlsx**

Supplementary T2

Click here to download Supplementary material for online publication only: Table S2.xlsx

Supplementary S1

Supplementary S2

Click here to download Supplementary material for online publication only: Fig S2 SEM_E_05_MgCaAl_RGB.pdf

Supplementary S3

Click here to download Supplementary material for online publication only: Fig S3 SEM_F_06_MgCaAl_RGB.pdf

**Supplementary S4**

Supplementary S5

**Supplementary S6**

Click here to download Supplementary material for online publication only: Fig S6 Sample 9_stitched-hires-crop.pdf